Liquid Crystals
Publication details, including instructions for authors and subscription information:
http://www.informaworld.com/smpp/title~content=t713926090

Linear and non-linear liquid crystal materials, electro-optical effects and surface interactions. Their application in present and future devices

Martin Schadt[a]
[a] Department RLCR, F. Hoffmann-La Roche Ltd., Basel, Switzerland

To cite this Article Schadt, Martin(1993) 'Linear and non-linear liquid crystal materials, electro-optical effects and surface interactions. Their application in present and future devices', Liquid Crystals, 14: 1, 73 — 104
To link to this Article: DOI: 10.1080/02678299308027305
URL: http://dx.doi.org/10.1080/02678299308027305

LIQUID CRYSTALS, 1993, VOL. 14, NO. 1, 73–104

Plenary Lecture

Linear and non-linear liquid crystal materials, electro-optical effects and surface interactions

Their application in present and future devices

by MARTIN SCHADT

F. Hoffmann-La Roche Ltd., Department RLCR,
4002 Basel, Switzerland

The structural, material and electro-optical properties of novel, halogenated nematic liquid crystals which contain quite different functional groups are correlated. Synergisms which lead to broad mesophases, low viscosities and large dielectric anisotropies further improve the performance of actively and passively addressed, high information content liquid crystal displays. Some recent developments, such as operation of supertwisted nematic displays with not only linear, but also circularly polarized light, are included. A recently presented, efficient liquid crystal colour projection concept, whose functional elements, i.e. polarizers, filters and modulators, consist entirely of liquid crystal devices, is reviewed. Its circular polarizers and filters are made up of novel, negative dielectric anisotropic cholesteric liquid crystals designed such that, dislocation-free, optically uniform, planar textures result from electric field alignment. Novel, non-linear optical ferroelectric liquid crystals which exhibit very large and stable second order harmonic coefficients $d_{22} = 5\,\mathrm{pm\,V^{-1}}$ have the potential to be used in integrated optical devices, such as frequency converters and Pockels modulators. Photopolymerization of polymer-coated substrates with linearly polarized light is shown to induce anisotropic, uniaxial orientation of the polymer side chains without mechanical treatment. The resulting anisotropic dispersive surface interaction forces align adjacent liquid crystal molecules parallel. This new, photo-induced liquid crystal aligning technique renders the generation of azimuthal director patterns possible. It opens up interesting possibilities for realizing new optical and electro-optical devices, including hybrid and stereo liquid crystal displays.

1. Introduction

The rapid advancement of liquid crystal display technology towards very high information content displays is due to the discovery of electro-optical field effects on which liquid crystal displays are based, the successful search for liquid crystals with novel material properties and the development of the technological tools required to manufacture today's sophisticated liquid crystal displays. The fruitful interaction amongst these three areas constantly broadens the basic understanding of liquid crystals and rapidly expands their applicability.

With the advancement of liquid crystal display technology, spin-offs are created which open up new applications and possibilities within the field as well as in non-display related areas: one example is the development of the thin film transistor technology required for manufacturing actively addressed, high information content liquid crystal displays. Another new example is strongly non-linear optical ferroelectric liquid crystals designed for integrated optics devices. For the first time, stable and highly efficient non-linear optically active ferroelectric liquid crystal materials are presented at this conference [1]. Their second harmonic non-linear optical susceptibilities are comparably large with those of the best inorganic non-linear optical crystals. The performance of the new non-linear optically active ferroelectric liquid

0267–8292/93 $10·00

crystals will briefly be reviewed. For a recent review of the development of the liquid crystal display and liquid crystal material technologies, see [2, 3].

In the following, some recent developments on nematic and ferroelectric field effects made in our laboratories are reviewed. They include circularly polarized operating modes of twisted nematic [4] and supertwisted nematic liquid crystal displays [5] which lead in reflective configurations to improved multiplexibility and/or to shorter response times [6]. Circularly polarized liquid crystal display operating modes are interesting configurations for projectors such as those for the liquid crystal polarized colour projection concept presented recently [7]. In this context, novel, short pitch cholesteric liquid crystals with negative dielectric anisotropy $\Delta\varepsilon=(\varepsilon_{\parallel}-\varepsilon_{\perp})<0$ are shown to be planar alignable in electric fields, such that dislocation-free circular polarizers and optical filters become feasible.

For future thin film transistor addressable twisted nematic liquid crystal displays, liquid crystals are required with threshold voltages below 1·5 V, low rotational viscosities, broad nematic mesophases, as well as adjustable optical anisotropies. Such materials are prerequisites for reducing driver voltages and liquid crystal display costs. Crucial for low threshold nematics are large, positive dielectric anisotropies $\Delta\varepsilon\gg0$. Moreover, and despite $\Delta\varepsilon\gg0$, for thin film transistor twisted nematic liquid crystal displays the compounds must exhibit poor solubility for residual ions from the polyimide aligning layers and a very low residual conductivity. These conflicting and highly demanding requirements can so far only be approached with molecules whose polarity results from halogenated groups that are combined with non-polar, low viscous structures [8–10]. Synergisms which result from combining different polar and linking groups, different rings and side chains in new, halogenated alkenyl liquid crystals are presented. Their favourable material properties for thin film transistor addressed twisted nematic liquid crystal displays, fast responding supertwisted nematic liquid crystal displays and short pitch cholesteric filters are compared with the material properties of known structures.

Planar, uniaxial alignment of liquid crystals over macroscopic areas *via* surface interactions is a prerequisite for inducing the macroscopic molecular configuration required to realize a specific electro-optical effect in a liquid crystal display. Virtually all of today's liquid crystal display substrates are coated with thermally polymerized thin films which are mechanically brushed to induce planar liquid crystal alignment. Because brushing is an integral process which generates uniform alignment over the entire substrate area [11], aligning patterns with different azimuthal angles ψ of the liquid crystal director $\mathbf{n}$ are not possible by this technique. Moreover, brushing generates dust particles and electrostatic surface charges which are both detrimental to high production yields in the manufacturing process of actively addressable liquid crystal display substrates. At the end of this plenary article a novel, light-induced, planar liquid crystal aligning technique is reviewed which we recently developed in collaboration with scientists from NIOPIK, Moscow [12]. Photopolymerization of polymer-coated liquid crystal display substrates with linearly polarized light is shown to induce uni-axial, planar alignment of liquid crystals without any mechanical treatment. The new linear photopolymerization liquid crystal aligning technique allows for the first time the generation of a liquid crystal director pattern with different azimuthal directions $\mathbf{n}$ (ψ) on the same substrate. This opens up a wide range of new electro-optical and optical applications not restricted to liquid crystal displays. Among them are hybrid liquid crystal displays which combine different electro-optical effects on the same liquid crystal display substrate, stereoscopic liquid crystal displays, or supertwisted nematic liquid crystal displays with *in situ* optical interference filters.

2. Influence of charge carriers on the performance of passively and actively addressed liquid crystal displays

Charge transport mechanisms in liquid crystals and the complex impedance of liquid crystal displays were recently shown to affect strongly not only the electro-optical performance of actively addressed twisted nematic liquid crystal displays, but also the frequency dependences of the optical appearance of passively addressed twisted nematic and supertwisted nematic liquid crystal displays [13]. Because modern, halogenated liquid crystal materials can be purified to the extent that their residual resistivity reaches values of high quality insulators, the investigation of transport mechanisms in liquid crystal layers over a broad range of resistivities becomes possible by selectively doping the liquid crystals with ionic impurities.

Figure 1 shows a simple equivalent circuit of a liquid crystal display picture element (pixel) from which the following exponential current decay $I(t)$ follows upon applying a voltage V_0

$$\left.\begin{aligned} I(t) &= I_\infty + I_0 \exp(-t/\tau), \quad \tau = \varepsilon_0 \frac{\varepsilon_a d + 2\varepsilon_{LC}\delta}{d/\rho_a + 2\delta/\rho_{LC}}, \\ I_\infty &= I(t=\infty) = V_0/(R_{LC} + 2R_a + R_{ITO}). \end{aligned}\right\} \tag{1}$$

The complex liquid crystal display impedance of the circuit in figure 1 implies that the actual voltage across the liquid crystal layer must depend on frequency

$$V_{LC}^2 = \frac{R_{LC}^2 ab^2 V_0}{[2R_a a + R_{LC} b + R_{ITO} ab]^2 + \omega^2 [2R_a^2 C_a a + R_{LC}^2 C_{LC} b]^2}, \tag{2}$$

where

$$a = 1 + (\omega R_{LC} C_{LC})^2; \quad b = 1 + (\omega R_a C_a)^2; \quad \omega = 2\pi f.$$

As a consequence also the voltage-induced deformation of the nematic director of the twisted nematic liquid crystal display and therefore its electro-optical signal depend on frequency and on the circuit parameters depicted in figure 1 [13]. From equation (2) follows that at low (< 10 Hz) and at high frequencies (> 10^4 Hz) the effective voltage across the liquid crystal layers decreases. At low frequencies, the decrease occurs when decreasing ρ_{LC} and/or by increasing the aligning layer thickness δ, whereas large ITO electrode resistivities cause the decrease at high frequencies. Frequency dependent variations of the voltage across the twisted nematic helix reduce the contrast of time multiplexed liquid crystal displays.

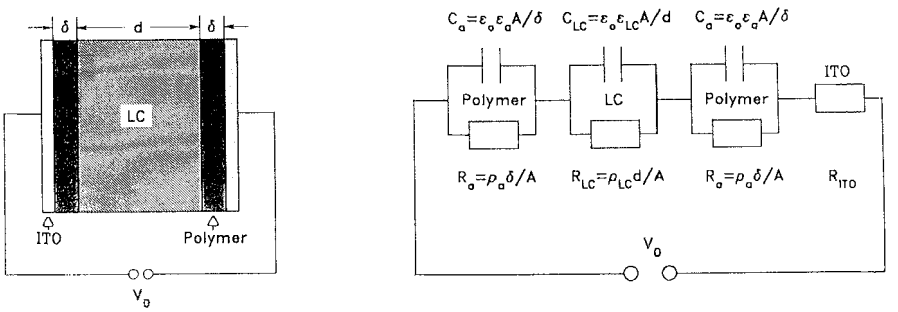

Figure 1. Schematic of a twisted nematic liquid crystal display and its linear equivalent circuit.

For various aligning layer resistivities ρ_a and layer thicknesses δ (see figure 1), as well as over six decades of liquid crystal resistivities $10^6\,\Omega\mathrm{m} \leqslant \rho_{LC}V \leqslant 10^{12}\,\Omega\,\mathrm{m}$ we have shown that the simple exponential decay of equation (1) is valid only within a conductivity regime A characterized by the product $\rho_{LC} < 10^9\,\Omega\,\mathrm{m}V$. In a second regime B, where $\rho_{LC}V > 10^9\,\Omega\,\mathrm{m}V$, space charge limited currents occur which are not simulated by the linear equivalent circuit of figure 1 [13]. As a consequence markedly different time dependences of the pixel current result in the two regimes A and B upon applying a voltage V_0. This is shown in figure 2 where the normalized pixel current follows the single exponential decay of equation (1) only in regime A. In the highly resistive regime B a transient current peak occurs which is due to the build-up of space charge within the liquid crystal layer. Space charge formation is caused by the rapid depletion of the low charge carrier density in the centre of the low conductivity liquid crystal layer (see figure 1) upon application of a voltage to the liquid crystal display. Because highly resistive liquid crystal materials are crucial for the realization of actively addressed liquid crystal displays, time dependent space charge effects have to be taken into account when evaluating the electro-optical liquid crystal display response and the effective liquid crystal resistivity of thin film transistor addressed liquid crystal displays.

Figure 3 schematically shows an actively addressed twisted nematic liquid crystal display (upper left) and the schematic time response $V(t)$ of the voltage across a pixel upon application of a pulse V_0 to the liquid crystal layer *via* the source of a thin film transistor (upper right). The video frame rate after which the optical information is refreshed is $T/2 = 20\,\mathrm{ms}$. The prerequisite for ideal preservation of the optical twisted nematic signal during the frame time is a constant voltage holding ratio $V(T/2)/V_0 = 1$ which corresponds to $\rho_{LC} = \infty$ in figure 1. However, in actual liquid crystal displays with finite values of ρ_{LC} and because of the different conductivity regimes A and B, not only the current response differs in the two regimes (see figure 2), but also the time dependence of the holding ratio $V(T)/V_0$. This is shown at the bottom of figure 3 [13]. From figure 3 it follows that the holding ratio in regime A obeys the same single exponential decay as the current in equation (1). However, in the highly resistive thin film transistor regime B, the holding ratio exhibits a biexponential decay. The fast

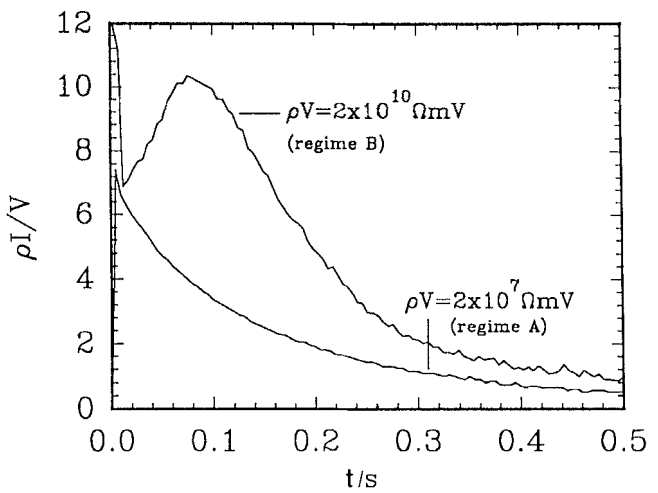

Figure 2. Normalized liquid crystal display currents in the conductivity regimes A and B in the isotropic phase.

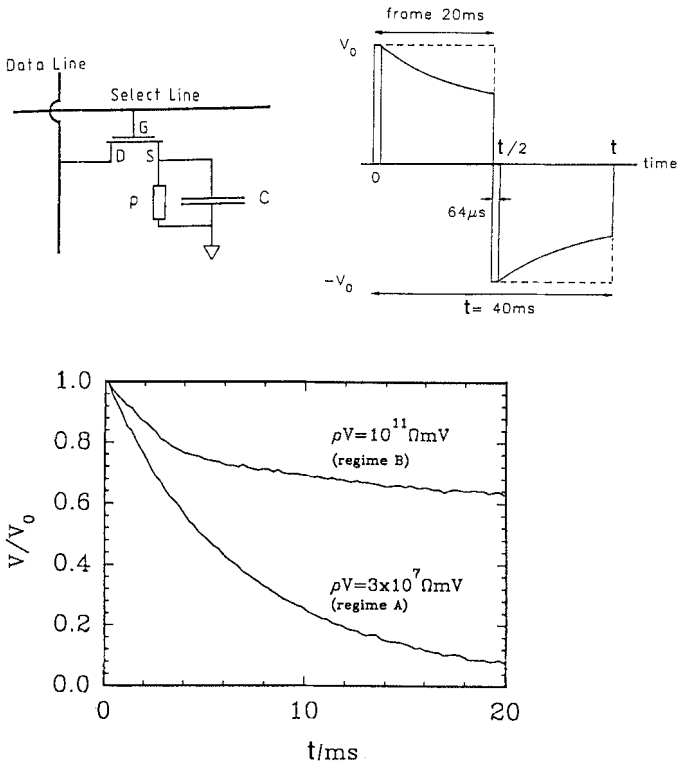

Figure 3. Upper left: thin film transistor addressed twisted nematic liquid crystal display pixel represented by parallel ρ_{LC} and C_{LC}. Upper right: schematic time response of the voltage across C_{LC} during the TV frame time $T/2$ upon application of a voltage pulse V_0 for 64 μs. Bottom: time dependence of the pixel holding ratio V/V_0 in the conductivity regimes A and B.

initial decay in figure 3 is caused by the fast build-up of space charge in the liquid crystal layer (see peak in graph B of figure 2). After the most mobile residual ions are removed from the bulk of the liquid crystal layer, that is, the build-up of space charge is essentially completed, the holding ratio decays much slower (see graph B in figure 3). Therefore, the decay of the holding ratio in regime B is much less pronounced within the frame time T than in regime A. The same applies to the decay of the optical signal of the twisted nematic liquid crystal display. From figure 3 and the dependence of the holding ratio on the product $\rho_{LC}V$, it follows that large holding ratios in thin film transistor twisted nematic liquid crystal displays not only require highly resistive liquid crystal materials, they also increase with increasing thin film transistor driving voltage V.

3. Structure–material properties of novel liquid crystals for thin film transistor addressed twisted nematic liquid crystal displays and cholesteric filters

We have shown before, for instance in [10, 14], that the introduction of double bonds at specific terminal chain positions of alkenyl liquid crystals markedly broadens the range of material properties of liquid crystals. Especially the elastic constants, the splay/bend elastic constant ratio k_{33}/k_{11}, the visco-elastic ratio γ_1/κ of rotational

viscosity γ_1 and elastic expression $\kappa = [k_{11} + (k_{33} - 2k_{22})/4]$, the mesomorphic temperature ranges, as well as the dielectric and optical anisotropies are affected. The synergisms which result from attaching different alkenyl end chains to different aromatic and non-aromatic rings of the rigid core of liquid crystal molecules, in combination with different polar groups, were shown to strongly expand the range of material properties of nematics, thus improving the performance of supertwisted nematic and twisted nematic liquid crystal displays [14]. Here some new structures are presented [15]. The properties of these thin film transistor compatible compounds are shown to be due to synergisms between selective structural elements. The new liquid crystals exhibit low viscosities, and they cover a broad range of dielectric and optical anisotropies, combined with pronounced nematic phases. Moreover, they exhibit large specific resistivities ρ_{LC} and low solubilities for residual ions in aligning layers.

3.1. *Positive dielectric nematics*

As an example, figure 4 shows the structure of one of the new, halogenated alkenyls. Their rigid cores contain different rings and linking groups. Moreover, different terminal chains and different polar groups are used. The structural elements and their (additive) nomenclature are depicted in figure 5. The nomenclature is analogous to that described earlier [14].

Figure 6 depicts the new liquid crystal materials. Permanent dipole moments due to aryl-F and aryl-Cl groups essentially determine the desired positive dielectric anisotropies. The appropriate introduction of dioxane rings serves the same purpose. Medium to large optical anisotropies result from linearly combining aromatic structural elements, such as benzene rings and C≡C-bonds (tolanes). To render comparisons as relevant as possible, all of the (short) alkyl and alkenyl side chains in figure 6 contain the same number (3) of carbon atoms. The systematic structural changes that were found to lead to synergisms are designated from top to bottom by dashed squares (see figure 6). The three top structures $1d_1CCPF$, $1d_1CCP_FF$ (10) and $3CCP_FF$ (8) serve as references. Comparing the application relevant nematic–isotropic transition temperatures T_c of the first five, directly linked structures at the top of figure 6 shows that the introduction of a double bond d in the 1-position (d_1) increases T_c by $\sim 45°C$. Another increase by $\sim 35°C$ results from replacing the *para*-fluorine F by Cl; whereas lateral fluorination depresses T_c by $\sim 35°C$. A depression of T_c also results from replacing the central cyclohexane ring C by a benzene ring P. Thus, the introduction of end chain double bonds in proper positions and the replacement of *para*-fluorine by

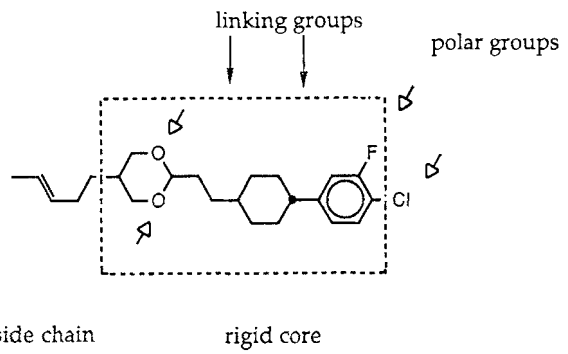

Figure 4. Example of halogenated, positive dielectric anisotropic nematic liquid crystal.

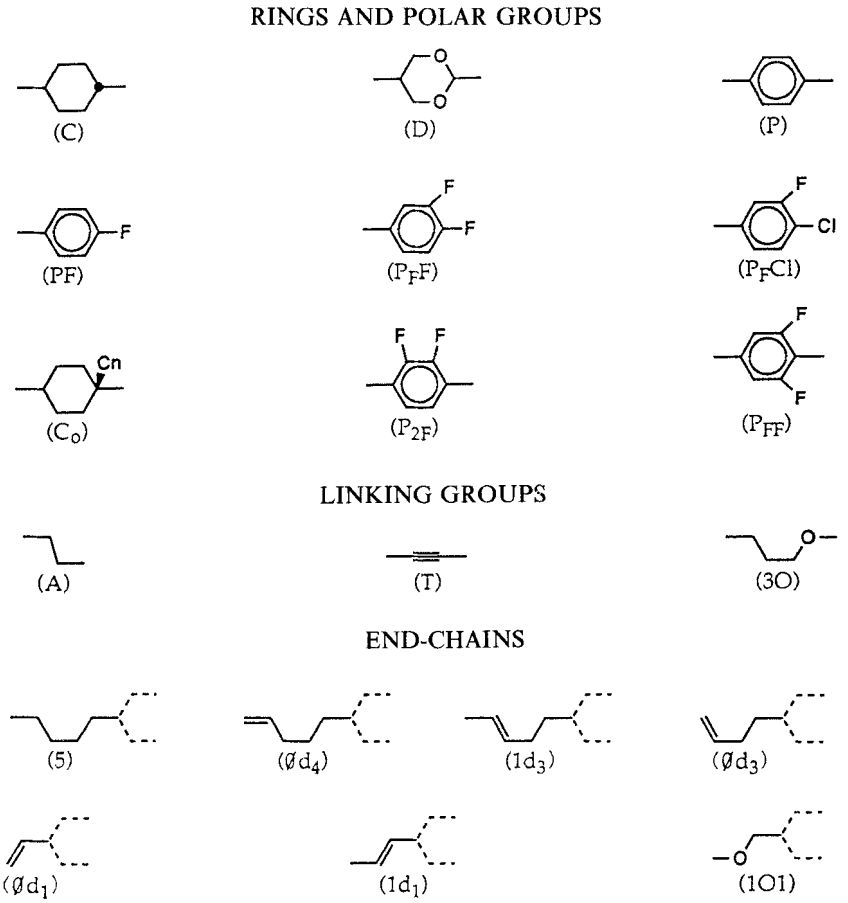

Figure 5. Structural elements and their nomenclature.

chlorine strongly increase T_c. This synergism is used in $1d_1DCP_FCl$ (see figure 6) to compensate the T_c depressing tendencies of its dioxane ring and its lateral F [10]. As expected, the replacement of *para*-F by Cl only slightly reduces the dielectric anisotropy $\Delta\varepsilon$ (see figure 6).

We have shown earlier that the proper distribution of structural elements with rather small permanent dipole moments at different molecular sites leads to large dielectric anisotropies and reduces the ion solubilization of the liquid crystal [10]. The para-chlorinated compound $1d_1DCP_FCl$ in figure 6 with $\Delta\varepsilon = 10$ is a new example using this approach.

The three compounds at the bottom of figure 6 all contain the dilaterally fluorinated benzene ring P_{FF} whose permanent C–F moments contribute to the positive dielectric anisotropy of the terminal ring P_FF. Of course the proper dielectric design of a liquid crystal is not sufficient to render the compound applicable. Especially in case of three ring structures, with their increased viscosities compared with two ring analogues, the compounds should exhibit a mesophase and a nematic–isotropic transition temperature above 100°C. We were therefore quite surprised and disappointed when we found that the directly linked $3CP_{FF}P_FF$ in figure 6 does not even exhibit a mesophase. Moreover, its pronounced monotropic transition temperature $T_c = -2$°C

Nomenclature	Structure	T_m/°C	T_c/°C	$\Delta\varepsilon(T_c-10°C)$	Ref.
$1d_1CCPF$ (ref)	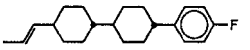	105	194	1·76	[10]
$3CCP_FF$	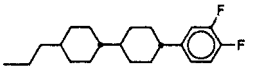	46	114	3·10	[8]
$1d_1CCP_FF$	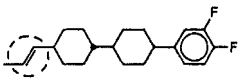	49	159	3·22	[10]
$1d_1CPP_FF$	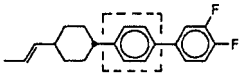	98	134	4·04	
$1d_1CCP_FCl$	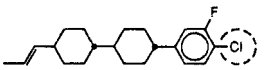	91	197	2·91	
$1d_1CCAP_FF$	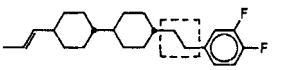	64	137	2·73	
$1d_1DCP_FCl$	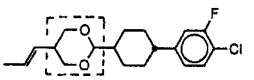	82	144	10·0	
$3CP_{FF}P_FF$	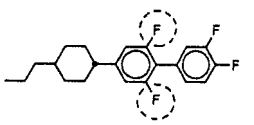	80	−2	–	
$3CP_{FF}TP_FF$	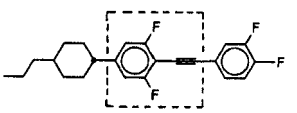	71	123	6·6	
$1d_1DP_{FF}TP_FF$	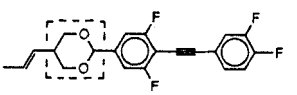	99	157	20·8	

Figure 6. Structures of reference (top three) and novel positive dielectric anisotropic halogenated nematic liquid crystals. T_m, T_c are melting and clearing temperatures. The dielectric anisotropy $\Delta\varepsilon=(\varepsilon_{\parallel}-\varepsilon_{\perp})$ of the individual compounds is determined at their respective reduced temperature $(T_c-10°C)=$constant.

is much too low for the design of mixtures (see figure 6). However, by sterically decoupling the rings P_{FF} and P_FF with a tolane linkage, a pronounced nematic phase was achieved. Simultaneously T_c strongly increased by 128°C (cf. $3CP_{FF}P_FF$ and $3CP_{FF}TP_FF$ in figure 6). Thus, it became possible to determine the influence of the new, synergetic structural element $P_{FF}T$ on $\Delta\varepsilon$: compared with $1d_1CPP_FF$ the dielectric anisotropy of $3CP_{FF}TP_FF$ increases by ~60 per cent (see figure 6). Moreover, replacing the cyclohexane ring C in $3CP_{FF}TP_FF$ by the comparably optically isotropic dioxane ring D strongly increases $\Delta\varepsilon$ further to 20·8 (see figure 6). To our knowledge $1d_1DP_{FF}TP_FF$ exhibits the largest dielectric anisotropy achieved so far in halogenated nematics. Comparably large $\Delta\varepsilon$s are known only for cyanopyrimidines [16] and laterally fluorinated cyano esters [17].

Table 1. Material data for binary mixtures of the halogenated nematics depicted in figure 6. Data in bold type determined at $T/T_c = 0{\cdot}8$ for the respective mixture, the others at $T = 22°C$. Optical anisotropy $\Delta n = (n_e - n_0)$, dielectric anisotropy $\Delta\varepsilon = (\varepsilon_{\parallel} - \varepsilon_{\perp})$, splay/bend elastic ratio k_{33}/k_{11}, elastic expression $\kappa = [k_{11} + (k_{33} - 2k_{22})/4]$, rotational viscosity γ_1, bulk viscosity η, nematic–isotropic transition temperature T_c.

Liquid crystal mixture		Δn	$\Delta\varepsilon$	k_{33}/k_{11}	$\kappa/10^{-12}$ N	γ_1/cP	η/cP	V_{10}/V	T_c/°C
(ϕd$_1$CCPF, 1d$_1$CCPF)	M1	**0·095**	**2·44**	**3·2**	**15**	**25**	**3·6**	**3·5**	**168**
50 mol 50									
(ϕd$_1$CCP$_F$F, 1d$_1$CCP$_F$F)	M2	**0·093**	**5·34**	**3·0**	**12**	**53**	**8·1**	**2·2**	133
50 50		0·098	6·34	3·1	14	155	23	2·1	
(ϕd$_1$CCP$_F$Cl, 1d$_1$CCP$_F$Cl)	M3	**0·121**	**4·52**	**2·9**	**17**	**40**	**4·2**	**3·0**	172
50 50									
(ϕd$_1$CCP$_F$F, 1d$_1$CCAP$_F$F)	M4	**0·091**	**4·79**	**2·9**	**13**	**71**	**9·1**	**2·4**	123
50 50		0·095	5·47	3·1	14	165	23	2·3	
(ϕd$_1$CCP$_F$F, 1d$_1$DCP$_F$F)	M5	**0·091**	**13·4**	2·4	**11**	**138**	**21**	**1·4**	103
50 50		0·092	14·0	2·4	11	178	27	1·4	
(ϕd$_1$CPP$_F$F, 1d$_1$CPP$_F$F)	M6	**0·170**	**6·70**	**2·1**	**11**	**~150**	**~15**	**2·2**	105
50 50		0·172	6·90	2·1	12	~210	~20	2·2	
(ϕd$_1$CCP$_F$F, 1d$_1$DP$_{FF}$TP$_F$F)	M7	**0·167**	**24**	**2·1**	**10**	**95**	**14**	**1·1**	117
50 50		0·172	27	2·2	11	207	25	1·1	

Table 1 shows the optical, dielectric (static), elastic and viscous properties of binary mixtures of the compounds from figure 6. Also depicted are the twisted nematic threshold voltages V_{10} (at 10 per cent transmission), determined for 6 μm twisted nematic liquid crystal displays. A summary of the measuring techniques is given in [14]. The data in bold type were determined at the respective reduced mixture temperatures $T/T_c = 0{\cdot}8$; the others are room temperature data (22°C). In those cases where the melting temperatures are above 22°C, extrapolated values are used if possible. They follow from the temperature dependence of the respective material parameters. Except for the rotational viscosity γ_1 and the bulk viscosity η, the material parameters and V_{10} in table 1 scale with the nematic order parameter S (T) [14]. Therefore, comparisons of Δn, $\Delta\varepsilon$, k_{33}/k_{11}, κ and V_{10} are made at constant reduced temperature $T/T_c = 0{\cdot}8$ (bold type); γ_1 and η are compared at 22°C. The top two mixtures M1 and M2 in table 1 consist each of the low viscosity, mono- and difluoro-homologous alkenyls described earlier [10], (see figure 6). Thus, they are typical representatives of their respective liquid crystal class and serve as references. Like M1 and M2, M3 and M6 too are made up of homologues, whereas the other mixtures each comprise 50 per cent of the common reference compound ϕd_1CCP_FF used in M2.

From table 1, it follows that: (i) Large dielectric anisotropies and rather low elastic expressions κ are achieved with $1d_1DP_{FF}TP_FF$ (M7). Both parameters strongly reduce the threshold voltage of twisted nematic liquid crystal displays [2]; (ii) the low rotational viscosity γ_1 of directly linked Xd_1CCP_FF compounds virtually does not increase when replacing $1d_1CCP_FF$ in M2 by the ethane linked $1d_1CCAP_FF$ (M4) or even by the considerably more strongly polar $1d_1DCP_FF$ (M5). In this context it is very interesting to note in table 3 that (iii), despite the dramatic reduction of threshold voltage V_{10} by $1d_1DP_{FF}TP_FF$, γ_1 of M7 remains surprisingly small. Both, the large dielectric anisotropy and the low γ_1 of M7 indicate that lateral difluoro-substitution leads in the case of $1d_1DP_{FF}TP_FF$ to a suppression of antiparallel molecular association [18]. The same mechanism is likely to contribute to the large $\Delta\varepsilon$ and the low γ_1 of $1d_1DCP_FF$ in M5; (iv) an increase in the optical anisotropy by ~ 20 per cent results when replacing *para*-fluorine by chlorine (cf. M2, M3); (v) the structural element $P_{FF}TP_FF$ in $1d_1DP_{FF}TP_FF$ strongly increases the optical anisotropy to values exceeding those of pure biphenyl cores (cf. M6 and M7; note the 100 per cent biphenyl contribution PP in M6 and the 50 per cent contribution in M7).

3.2. *Non polar and negative dielectric nematics*

Three ring compounds alone do not allow us to achieve optimally short response times and other properties which are prerequisites for realizing advanced super twisted nematic or thin film transistor addressed twisted nematic liquid crystal displays [2]. Moreover, for applications where non-polar or negative dielectric anisotropic liquid crystals are required, different structures from the above are needed.

Figure 7 shows some new, non-polar (top) nematic liquid crystals as well as two negative dielectric anisotropic (bottom) nematics with phase transition temperatures and dielectric anisotropies $\Delta\varepsilon$ $(T_c - 10°C)$. A common feature of all of them is their very low viscosities combined with pronounced nematic phases (except for the low viscosity, positive dielectric anisotropic dopant ϕd_3CPCl which is monotropic). In contrast to ϕd_1CC5, 3CPT1 exhibits a large optical anisotropy. The negative dielectric anisotropy of $5CC_0d_3\phi$ in figure 7 follows from its lateral C≡N dipole moment, whereas that of $3CC3OP_{2F}O_2$ is due to dilateral fluorination combined with a

Nomenclature	Structure	T_m/°C	T_{SN}/°C	T_c/°C	$\Delta\varepsilon(T_c-10°C)$	Ref.
$3CPOd_31$ (ref)	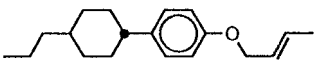	42		57	−0·27	[2]
ϕd_1CC5	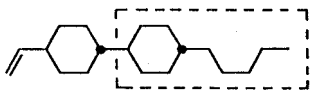	−8	52	63	0·17	[10]
3CPT1	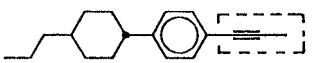	45		55	0·40	
ϕd_3CPCl	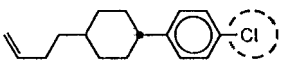	22		−10	—	
$5CC_0d_3\phi$	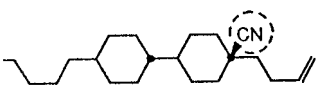	26		61	−5·0	
$3CC3OP_{2F}O2$	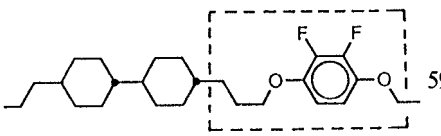	59		135	−3·5	[19]

Figure 7. Structures, transition temperatures and static dielectric constants of novel, low viscosity, non-polar and negative dielectric anisotropic nematic liquid crystals.

basically non-aromatic rigid core. $3CPOd_31$ at the top of figure 7 is a low viscosity reference compound of medium optical anisotropy [10, 14].

Table 2 shows the material properties of binary mixtures comprising the compounds of figure 7 and $3CPOd_31$. The data in bold type were determined at the respective reduced mixture temperatures ($T_c-10°C$); the others are room temperature data (22°C). Because of the narrower nematic ranges of two ring compounds, comparisons as far below T_c as $T/T_c=0{\cdot}8$, as in table 1, were not possible. Due to the small dielectric and diamagnetic anisotropies of some of the binary mixtures in table 2, the accurate determination of the rotational viscosities proved to be difficult [14].

Table 2 shows that the rotational viscosities γ_1 of the non-polar mixtures M8 and M9 are indeed very small, i.e. $\gamma_1(22°C)<35$ cP. The same holds for their bulk viscosities $\eta(22°C)\leqslant 12$ cP. Also doping $3CPOd_31$ with the positive dielectric dopant ϕd_3CPCl causes γ_1 to decrease from 86 cP to 29 cP, while simultaneously inducing a positive dielectric anisotropy, leading to V_{10} ($T_c-10°C$) = 2·9 V in M10 (see table 2). In the context of positive dielectric mixtures, it is interesting to compare M11 in table 2 with M2 in table 1: combining ϕd_1CCP_FF with the low viscosity, non-polar ϕd_3CC3 in M11 leads to a drastic γ_1 reduction from γ_1 (M2) = 155 cP to γ_1 (M11) = 59 cP, i.e. even below γ_1 of the low viscosity reference compound $3CPOd_31$ (see table 2). This illustrates that indeed very small viscosities, low thresholds and high T_c values can be achieved by suitably combining the halogenated compounds in figure 6 with the non-polar liquid crystals in figure 7.

Table 2. Material parameters for mixtures consisting of the low viscosity, non-polar or negative dielectric anisotropic compounds depicted in figure 7. Data in bold type determined at ($T_c - 10°C$) of the respective mixture, the others at 22°C.

Liquid crystal mixture		Δn	$\Delta\varepsilon$	k_{33}/k_{11}	$\kappa/10^{-12}$ N	γ_1/cP	η/cP	V_{10}/V	T_c/°C
3CPOd$_3$1 (100%, ref)		**0·089**	**−0·27**	**1·2**	**9**	**22**	**5·3**	—	**57**
						~86	**~13**		
(ϕd$_1$CC5, 3CPOd$_3$1)	M8	**0·061**	**−0·01**	**1·1**	**7**	**<25**	**5·2**	—	**54**
50 50		0·076	−0·03	1·1	12	<35	10		
(3CPT1, 3CPOd$_3$1)	M9	**0·112**	**0·05**	**1·3**	**9**	**~15**	**6·4**	—	**54**
50 50		0·137	0·04	1·4	16	~25	12		
(ϕd$_3$CPCl, 3CPOd$_3$1)	M10	**0·091**	**1·19**	**1·2**	**8**	**41**	**12**	**2·9**	**28**
50 50		0·084	1·09	1·2	6	29	11	2·7	
(ϕd$_1$CCP$_F$F, 0d$_3$CC3	M11	**0·072**	**2·44**	**1·7**	**13**	**76**	**15**	**2·6**	**88**
50 50		0·072	2·35	1·7	13	59	12	2·6	
(5CC$_0$d$_3$0, 3CPOd$_3$1)	M12	**0·074**	**−1·28**	**1·1**	**8**	**31**	**7·3**	—	**51**
20 80		0·090	−1·64	1·2	13	85	16		
(3CC3OP$_{2F}$02, 3CPOd$_3$1)	M13	**0·085**	**−1·27**	**1·2**	**10**	**24**	**5·1**	—	**73**
20 80		0·110	−2·18	1·4	22	164	19		

It is interesting to note that the negative dielectric anisotropies of M12 and M13 in table 2 are almost identical, despite the different $\Delta\varepsilon$ values of their components (see figure 7). This indicates that not only dilateral fluorination of the type P_{FF} (see figure 6) reduces antiparallel molecular association, but also P_{2F} (see figure 7). For strongly negative dielectric anisotropic compounds which are usually highly viscous, the viscosities of $5CC_0d_3\phi$ and $3CC3OP_{2F}O2$ in M12 and M13 are low (see table 2). Compounds of this type are used in dislocation-free optical cholesteric filter mixtures described below and in mixtures designed for DAP liquid crystal displays [20].

4. Liquid crystal display projection with cholesteric filters/polarizers; circular polarized operation of supertwisted nematics

4.1. *Liquid crystal display projection with cholesteric filters/polarizers*

Recently we have shown that unpolarized light can efficiently be converted into circularly or linearly polarized light via selective reflection at cholesteric liquid crystal filters [21]. Moreover, a liquid crystal polarized colour projection concept was presented whose functional parts consist of cholesteric liquid crystal filters/polarizers and liquid crystal display modulators [7]. The modulators can be based on a number of different field effects. Liquid crystal polarized colour projectors effectively convert incoherent, unpolarized white input light into the three circularly polarized basic colours blue, green and red. Figure 8 shows an example of one stage of a liquid crystal polarized colour projector which comprises a twisted nematic liquid crystal display modulator operated in reflection. Combining the liquid crystal polarized colour projection concept with the microlens optics recently presented by Sharp [22] could improve the brightness of liquid crystal display projectors by at least a factor of two.

Figure 9 shows the fundamental optical properties of planar cholesteric liquid crystal layers [23]. Within the wavelength range $\Delta\lambda$ where Bragg reflection occurs, incident, incoherent and unpolarized light of intensity $I_0 = (I_0^-/2 + I_0^+/2)$ is partly reflected and partly transmitted by the left handed cholesteric filter CF_L [7].

Figure 10 shows the selective reflection of unpolarized light at vertical incidence on to a left handed cholesteric filter CF_L. The pitch of the filter is adjusted such that maximum selective reflection for left handed light occurs at $\lambda_0 = 600\,\text{nm}$. The right handed polarization passes the filter unaffected over the entire visible wavelength range

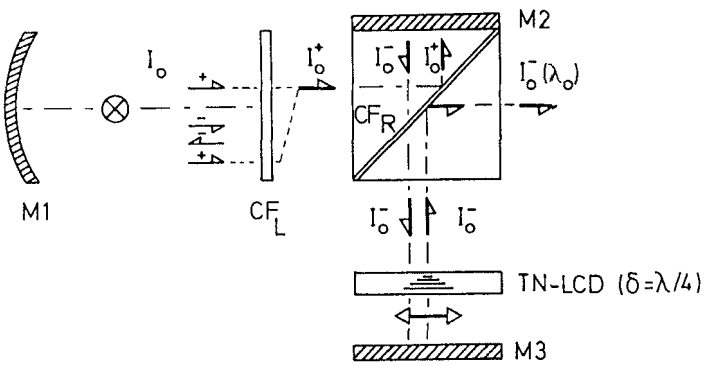

Figure 8. Principle of one stage of a liquid crystal polarized colour projection operated in reflection. The optical retardation of the twisted nematic liquid crystal display in the off-state is $\delta\,(V=0) = \lambda/4 \cdot (2n+1)$. The left handed circularly polarized output intensity I_0^- at wavelength λ_0 can be further selectively deflected at a right handed cholesteric filter CF_R (not shown in the drawing). M1, M2, M3 = metallic reflectors, CF_L = left handed cholesteric filter whose wavelength of selective reflection λ_0 is tuned to that of CF_R.

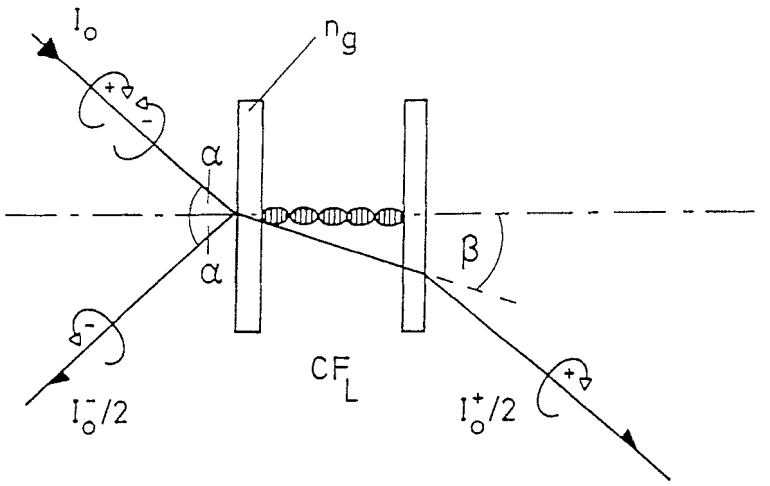

$$\lambda_0 = \frac{n_o + n_e}{2} p = \bar{n} p, \tag{3}$$

$$\lambda(\alpha) = \lambda_0 \cos\left[\sin^{-1}\left(\frac{2\sin\alpha}{n_o + n_e}\right)\right], \tag{4}$$

$$\Delta\lambda = \lambda_0 \Delta n/\bar{n}, \tag{5}$$

$$\sin\alpha/\sin\beta = n_g. \tag{6}$$

Figure 9. Optical properties of planar cholesteric filters. λ_0 = wavelength of selective reflection, p = cholesteric pitch, $\Delta\lambda$ = bandwidth of selective reflection/transmission. I_0^- and I_0^+ are the left and right handed circularly polarized light intensities, I_0 = unpolarized input light.

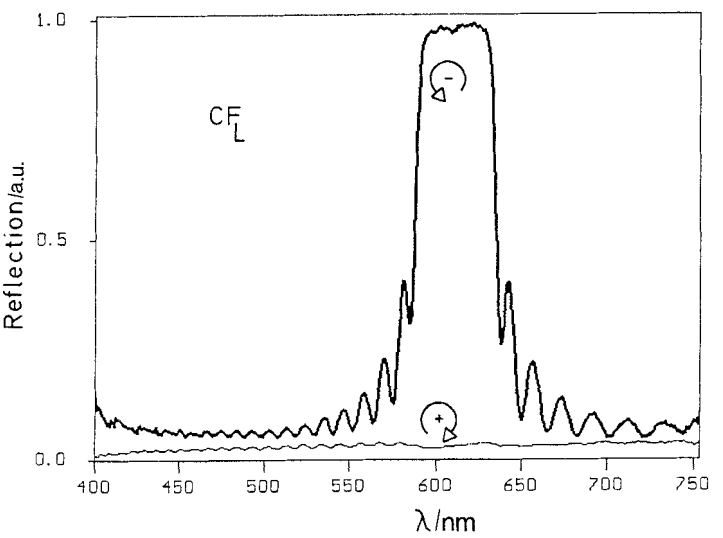

Figure 10. Wavelength dependence of selective reflection of unpolarized light at vertical incidence on to a left handed, planar cholesteric layer. The short pitch cholesteric liquid crystals are from F. Hoffmann-La Roche.

(see figure 10). The cholesteric liquid crystals and the filter substrate preparation are described in [7]. The measurements in figure 10 show that non-absorbing, high quality optical filters/ polarizers can be realized provided uniform planar cholesteric layers are achieved.

A prerequisite to realize the liquid crystal polarized colour projection concept are cholesteric filter materials whose helical axes are uniaxially alignable on transparent substrates. Any dislocations which occur, for instance during the filling process of the filter cell or upon rapidly cooling the filters from the isotropic into the cholesteric phase, induce light scattering and reduce the polarization efficiency of the filters [7]. To cure focal-conic dislocations in cholesteric layers we developed short pitch, negative dielectric anisotropic cholesteric liquid crystals which can be planar aligned by external electric fields. The effect of field alignment is demonstrated in the micro-photographs of figure 11. They show a negative dielectric anisotropic cholesteric layer with selective reflection at $\lambda_0 = 470$ nm sandwiched between two glass plates partially coated with ITO electrodes. The top photograph shows the numerous depolarizing dislocations in the filter which occur during the filling process. The bottom photograph shows the same filter after a voltage of 10 V μm^{-1} was applied to the segmented electrode for 20 s. Due to field alignment an optically perfectly planar cholesteric texture results over the entire electrode area. Outside the electrode area the dislocations remain (see figure 11). After switching the aligning field off, the dislocation-free, optically uniform configuration remains stable.

4.2. *Circularly polarized operation of supertwisted nematic liquid crystal displays*

Figure 12(*a*) shows the conventional, linearly polarized transmissive operating mode of super twisted nematic liquid crystal displays. Figures 12(*b*) and (*c*) are two recently presented, circularly polarized operating modes [6]. The three configurations are adjusted such that positive contrast results, i.e. they are transmissive in their off-states and non-transmissive in their on-states. Two supertwisted nematic liquid crystal displays with twist angles $\varphi = 180°$ and $\varphi = 240°$ were used to investigate the influence of φ on the transmission–voltage characteristics of circularly polarized supertwisted nematic modes. To adjust the polarization states depicted in figures 12(*b*) and (*c*), the supertwisted nematic liquid crystal displays were rotated around the axis of light propagation. Small deviations from maximum off-state transmission and/or reduced on-state extinction were compensated with the variable optical compensator C. Instead of positive contrast, a negative contrast can be achieved by simply replacing one of the left handed circular polarizing cholesteric filters CF_L in figure 12(*b*) by a right handed filter [7]. Alternatively, the optical off-state retardation δ (supertwisted nematic liquid crystal display + C) $= \delta(V=0) = n\lambda$, $n = 1, 2, \ldots$ can be changed to $\delta(V=0) = \lambda/2\,(2n+1)$, $n = 0, 1, \ldots$. In the configuration of figure 12(*c*), a reversal of contrast from positive to negative results when changing the optical retardation from $\delta\,(V=0) = \lambda/4(2n+1)$, $n = 0, 1, \ldots$ to $\delta(V=0) = \lambda/2\,(2n+1)$, $n = 0, 1, \ldots$.

We have shown [6] that the optical threshold voltages V_c of conventionally operated supertwisted nematic liquid crystal displays as well as of supertwisted nematic liquid crystal displays which are operated with circular polarizers are identical with the thresholds for mechanical deformation of the supertwisted helix

$$V_c = \pi\left[\frac{1}{\varepsilon_0 \Delta\varepsilon}\left\{k_1 + (k_3 - 2k_2)\left(\frac{\varphi}{\pi}\right)^2 + 2k_2\left(\frac{\varphi}{\pi}\right)\frac{2d}{p_0}\right\}\right]^{1/2}, \tag{7}$$

where φ = twist angle, p_0 = natural helical pitch, d = cell gap, k_i = elastic constants.

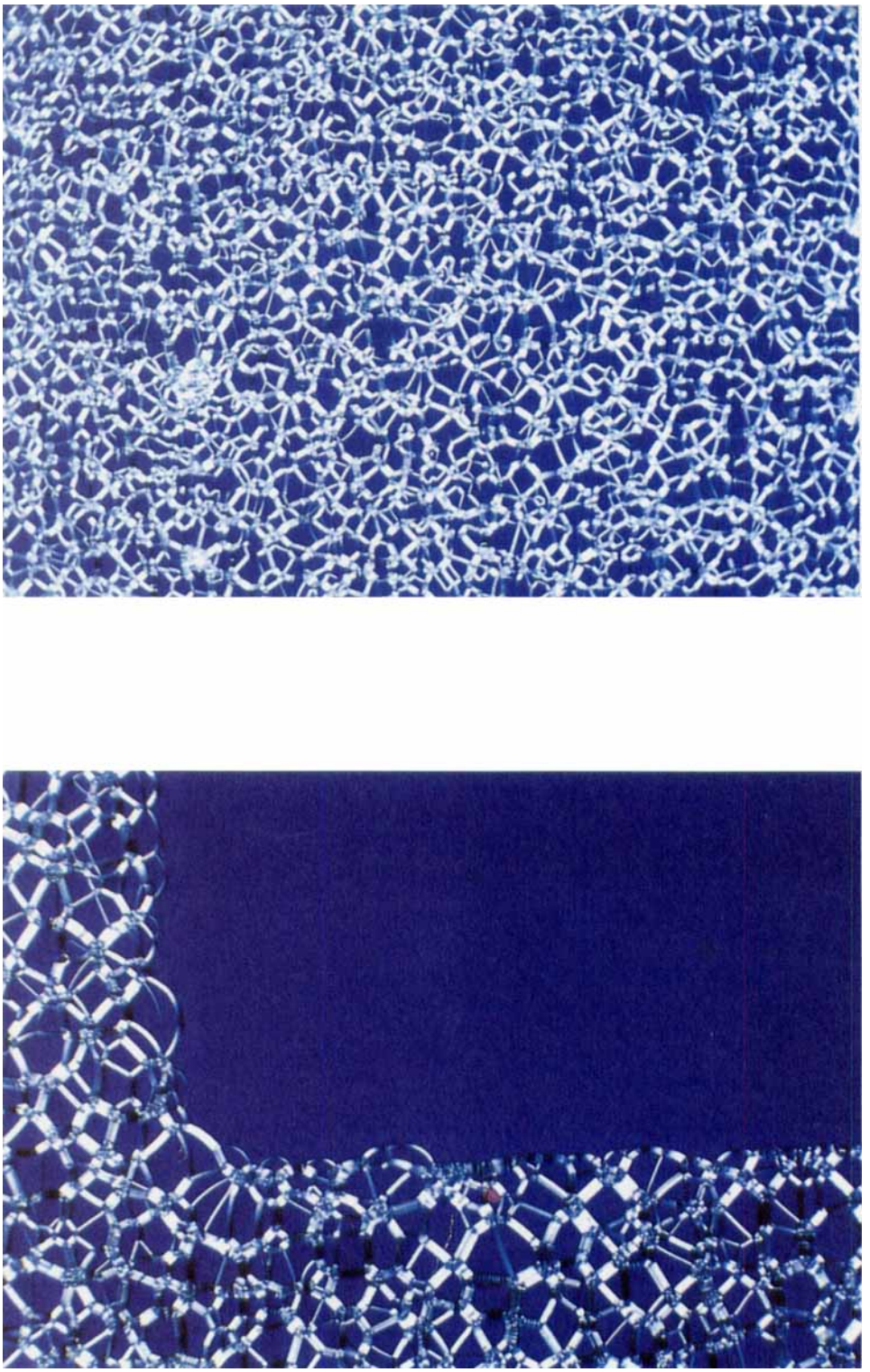

Figure 11. Electric field alignment of a cholesteric filter comprising a negative dielectric anisotropic liquid crystal from F. Hoffmann-La Roche. Top: before field alignment. Bottom: after having applied a field of 10 V μm^{-1} to the electrode-coated area of the filter; cell gap $d = 6\,\mu m$.

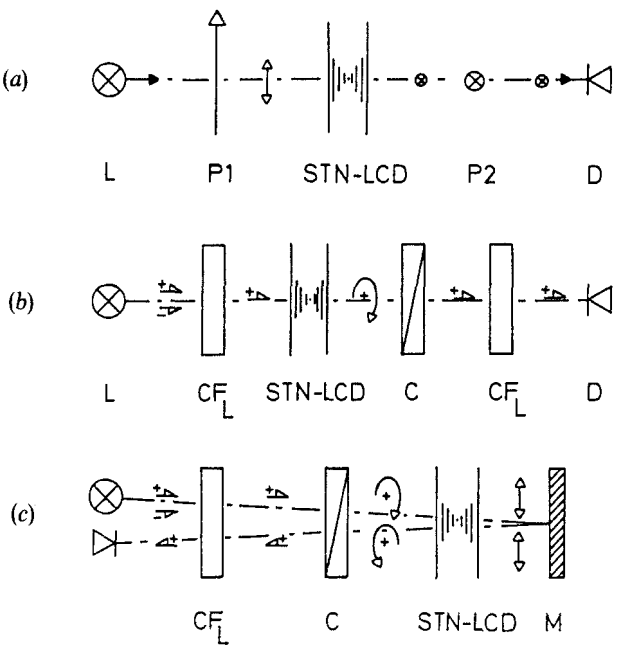

Figure 12. (*a*) Conventional, linearly polarized supertwisted nematic liquid crystal display operated in transmission. (*b*) New, circularly polarized transmissive supertwisted nematic liquid crystal display operating mode. (*c*) New, reflective, circularly polarized supertwisted nematic liquid crystal display operating mode. Both, the $\varphi = 180°$ and the $\varphi = 240°$ supertwisted nematic liquid crystal displays comprise mixture 6317 from F. Hoffmann-La Roche; cell gaps $d = 5{\cdot}95\,\mu$m.

Apart from a low threshold voltage, the steepness of the electro-optical-characteristics of a time multiplexed liquid crystal display should be as high as possible. The upper part of figure 13 shows the electro-optical characteristics of a $\varphi = 180°$ supertwisted nematic liquid crystal display operated in the two circularly polarized modes depicted in figure 12. The lower graphs in figure 13 are recordings of a $\varphi = 240°$ supertwisted nematic liquid crystal display. It is interesting to note in figure 13 that both reflective graphs exhibit considerably steeper characteristics than the conventional two polarizer configurations. In the case of the supertwisted nematic liquid display with $\varphi = 180°$, this improves the multiplexibility at full contrast 2·3 times, from N (transmission) $= 24 \rightarrow N$ (reflection) $= 56$ lines. With 240° twist, the multiplexibility improves 3·1 times from N (transmission) $= 507 \rightarrow N$ (reflection) $= 1600$; where the number of multiplexible lines N follows from [24]:

$$N = [(1+p)^2 + 1]^2 / [(1+p)^2 - 1]^2; \qquad p = \Delta V / V_c. \tag{8}$$

The considerably improved multiplexibility in reflection for a given supertwisted nematic geometry and with a given LC mixture cannot only be used to further increase the number of multiplexible lines of a supertwisted nematic liquid crystal display. Alternatively, the concept can also be applied to reduce the electro-optical response times of supertwisted nematic liquid crystal displays by operating them at lower twist angles while maintaining their multiplexing rate.

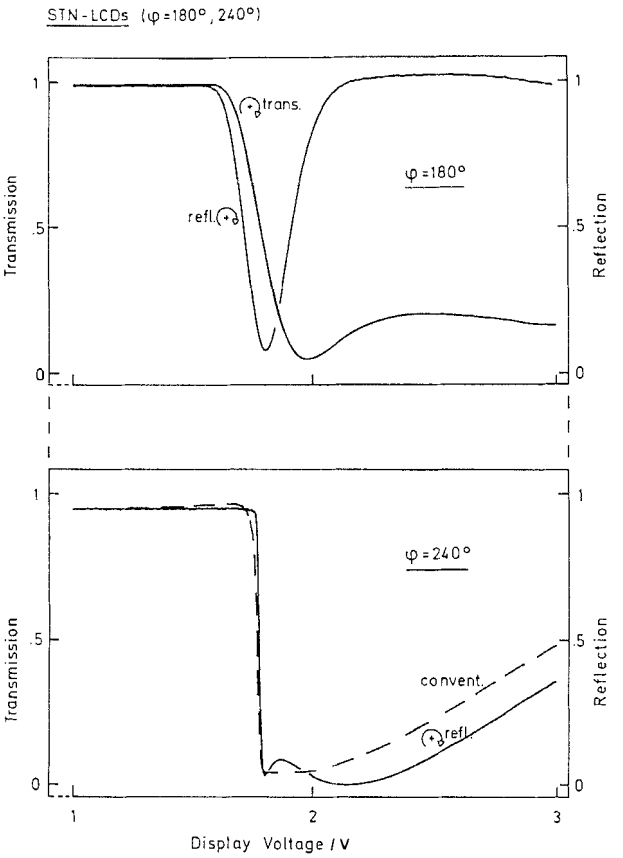

Figure 13. Electro-optical characteristics of $\varphi = 180°$ and $\varphi = 240°$ supertwisted nematic liquid crystal displays operated in the circularly polarized modes of figures 12(*b*) and (*c*).

Qualitatively, our findings can be explained as follows. Except for additional reflection losses, no optical changes occur between transmissive and reflective operation of conventional supertwisted nematic liquid crystal displays, i.e. in supertwisted nematic liquid crystal displays with linear entrance and exit polarizer. The slope of the electro-optical characteristics of conventional supertwisted nematic liquid crystal displays and thus their multiplexity are therefore identical in transmission and in reflection. This invariance can be broken when operating supertwisted nematic liquid crystal displays in a reflective configuration of the type depicted in figure 12(*c*). In this configuration, full use is made of the field-induced optical retardation properties of the supertwisted nematic helix on incident and reflected beams. The overall effective optical retardation of the helix doubles. As a consequence considerably steeper electro-optical characteristics and therefore improved multiplexibility result [6].

Because of the large optical off-state order n in which supertwisted nematic liquid crystal displays are operated in the reflective configuration of figure 12(*c*), a single linear polarizer can also be used instead of the circular polarizer CF_L.

5. Photoinduced parallel surface alignment of liquid crystals; liquid crystal display performance

Recently we have shown that photopolymerization of polymer-coated glass substrates with linearly polarized light leads to a uniaxial, planar orientation of the polymer molecules [12]. The linearly photopolymerized layers exhibit UV dichroism and optical anisotropy. Moreover, the resulting anisotropic dispersive surface interaction forces were shown to align adjacent liquid crystals parallel [12]. The new linearly photo polymerized aligning technique allows for the first time generation of a homogeneous liquid crystal director pattern $\mathbf{n}(\psi)$ with different azimuthal director angles ψ on the same substrate. No mechanical treatment is required.

5.1. *Linear photopolymerization of liquid crystal display substrates*

The generation of uniaxial alignment in liquid crystals either parallel (homogeneous) or perpendicular (homeotropic) to a solid substrate results from complex anisotropic surface anchoring interactions between substrate and liquid crystal. The alignment of the liquid crystal director $\mathbf{n}$ at the liquid crystal–substrate interface and the stability of the alignment are determined by the shape of the surface anchoring potential. In a microscopic picture, the following four contributions to the anchoring energy can be distinguished: topological, steric, polar and dispersive (van de Waals). Except for the topological part, all contributions are primarily governed by intermolecular interactions between substrate and liquid crystal.

The interfacial orientation of the director $\mathbf{n}$ is determined by the difference $\Delta\gamma$ between the anisotropic surface free energy of the liquid crystal and the interfacial free energy of the liquid crystal substrate. Since $\Delta\gamma$ is the small difference between two large numbers [25, 26] and because both, the free energy of the liquid crystal and the free energy of the interfacial layer are anisotropic quantities, $\Delta\gamma$ is in most practical cases very difficult to estimate. The problem is further complicated by the various and competitive mechanisms which contribute to the anchoring energy [27]. Moreover, very little is known about the specific intermolecular interactions at the interface and their anisotropies.

It was shown by Berreman [28] that grooved surfaces minimize the elastic deformation energy of nematics by forcing their directors $\mathbf{n}$ to align parallel to the grooves. By neglecting possible competing anchoring forces due to intermolecular interactions, Berreman showed that the grooved topology of surfaces, combined with the inherent tendency of nematics to minimize splay and bend elastic deformations induces homogeneous alignment.

As shown in § 3, virtually all liquid crystals designed for field-effect liquid crystal displays comprise permanent dipole moments, such as lateral or longitudinal cyano or halogen groups. Therefore, their alignment may be affected by dipolar interactions, with the substrate. However, since little is known about electric fields on free surfaces, the dipolar contribution to the surface energy which aligns the effective dipoles along the field is difficult to estimate. For methoxy benzylidene-butyl aniline, MBBA, Prost and Ter-Minassian-Saraga have experimentally determined the dipolar part of the surface energy of a surfactant-coated surface [25]. They attributed 25 per cent of the total surface energy to dipolar interactions, whereas 75 per cent was attributed to dispersive forces. The substrate coatings consisted of monomolecular layers of a polar surfactant containing a (non-polar) hydrocarbon side chain. Surfactant layers of different density were administered by Langmuir Blodgett techniques. In their evaluation, the authors did not consider possible steric contributions to the liquid

crystal alignment via the hydrocarbon side chains of the surfactant. Thus, possible chain reorientation and increasing chain rigidity with increasing surfactant density and/or the induction of flow alignment in the end chains during film preparation were neglected.

The boundary aligning layers of virtually all of today's liquid crystal displays which require homogeneously aligned liquid crystal–substrate interfaces are buffed polymer layers [11]. However, in contrast to the simplicity of this aligning process, the microscopic mechanisms which are responsible for the alignment are complex and have hardly been investigated as yet. This partly explains the often ambiguous interpretation of experimental results on buffed polymer layers. While some authors propose that the buffing process stretches the polymer chains, thus aligning the liquid crystal director parallel to the direction of buffing [29], others—such as Ishihara *et al.* [30]—have shown that the director orientation need not be parallel to the buffing direction. By scanning electron microscopy the same authors showed that buffing creates micro-grooves on polymer films which, however, do not seem to dominate topologically the liquid crystal alignment [30].

Okano and Murakami [26] as well as Bernasconi, Strässler and Zeller [31] have calculated the dispersive contribution $\Delta\gamma$ of an anisotropic liquid crystal L in contact with an isotropic substrate S to the total anchoring energy from the respective complex, principal dielectric functions. They derived the following expression for the anchoring energy between liquid crystal and an isotropic solid substrate [31]:

$$\Delta\gamma = \frac{\gamma'_{\perp} - \gamma'_{\parallel}}{\gamma_0} = A\frac{\Delta\alpha}{\alpha_{av}} + B\frac{\Delta\delta}{\delta}, \tag{9}$$

where $\gamma'_{\parallel}$ and $\gamma'_{\perp}$ are the planar and the homeotropic anchoring contributions. The rather elaborate coefficients A and B depend on the UV absorption frequencies ω_0 of liquid crystal and substrate. They also depend on the average liquid crystal polarizability $\alpha_{av} = (\alpha_{\parallel} + 2\alpha_{\perp})/3$ and on the (isotropic) polarizability α_s of the substrate. From equation (9), it follows that the optical anisotropy $\Delta n = (n_e - n_0)$ of the liquid crystal, as well as variations in the separation parameter δ, contribute to the anchoring energy. Because Bernasconi *et al.* assumed isotropic substrates for their calculations, anisotropic dispersive substrate terms, which are a prerequisite for uniaxial planar alignment, do not occur in equation (9).

We have shown that photopolymerization of substrates coated with polyvinyl-4-methoxycinnamate (PVMC) with linearly polarized UV light ($\lambda = 320$ nm) generates planar, uniaxial alignment in adjacent liquid crystals [12]. The nematic director aligns perpendicular to the polarization direction $P_{\parallel}$ of the linearly photopolymerization inducing **E** vector of the linearly polarized light. Figure 14 shows the mechanisms in the photopolymer which we assume in our model to lead to the uniaxial, planar, anisotropic van der Waals surface interactions which align the liquid crystal molecules [12]: (i) linear photopolymerization leads to a preferred depletion of cinnamic acid side chain molecules along $P_{\parallel}$ due to cross-linking; (ii) this causes an anisotropic distribution of the long axes of monomeric cinnamic acid molecules in the PVMC layer preferably perpendicular to $P_{\parallel}$. (iii) Linear photopolymerization creates an anisotropic distribution of cyclobutane molecules with their long axes also preferably aligned perpendicular to $P_{\parallel}$. From (ii) and because of their elongated (*trans*) shape, the cyclobutane molecules may by themselves exert an orienting effect on the hydrocarbon main chains to which they are attached. Figure 14 schematically depicts these three anisotropic molecular partial configurations which we assume to occur in linearly

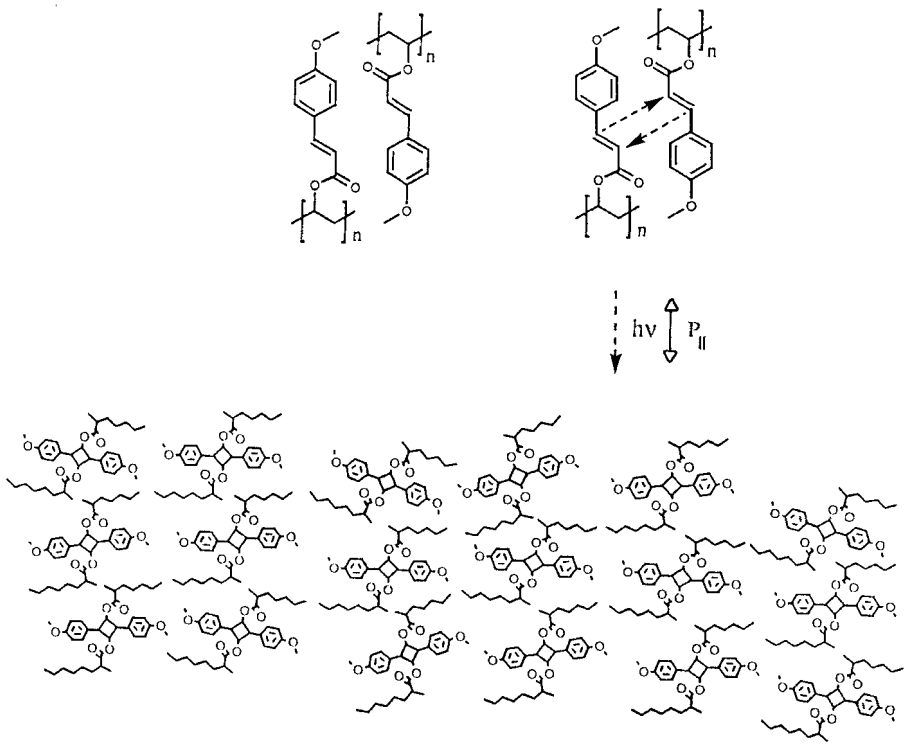

Figure 14. Schematic of the three anisotropic molecular configurations which we assume to occur in linearly photopolymerized PVMC films; $P_{\parallel}$ = UV curing polarization direction.

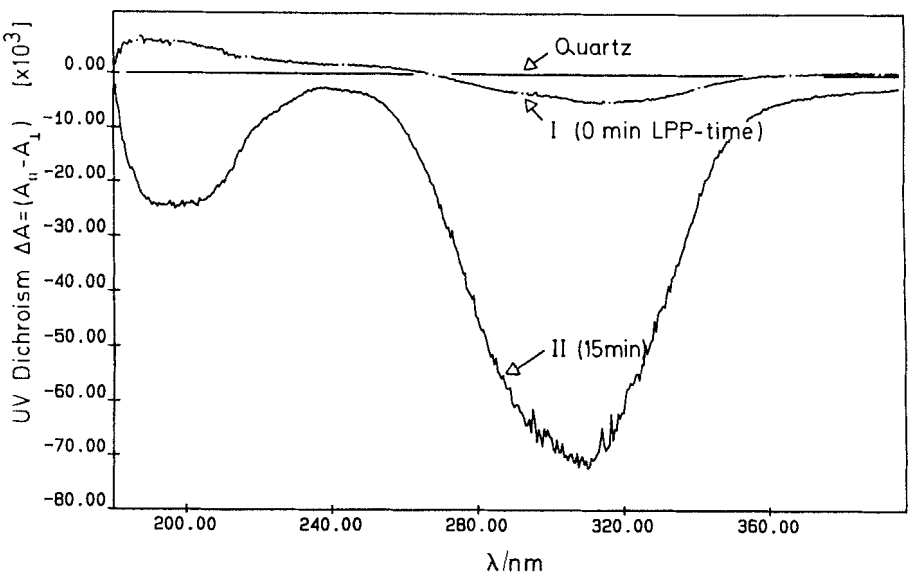

Figure 15. Dichroism $\Delta A = (A_{\parallel} - A_{\perp})$ of the UV absorption of a 100 nm thick PVMC film photopolymerized with linearly polarized light. Graph I: before linear photopolymerization; graph II: 15 min after linear photopolymerization.

photopolymerized PVMC substrates. Because all of these configurations exhibit a preferred longitudinal axis perpendicular to the linear polarization direction $P_{\parallel}$ of the UV curing light *hv* (see figure 14), synergisms can be expected to occur. These would amplify the individual homogeneous liquid crystal aligning properties of the partial molecular configurations in figure 14 [12].

Figure 15 shows the UV dichroism in a 100 nm thick PVMC film before (see graph I) and after 15 min of linear photopolymerization (see graph II) [12]. The direction of parallel film absorption $A_{\parallel}$ in $\Delta A = (A_{\parallel} - A_{\perp})$ is identical to the polarization direction of photopolymerization. After linear photopolymerization of the PVMC film, the initially isotropic absorption of the non-irradiated film becomes strongly negative dichroic at the wavelengths $\lambda_0 = 300$ nm and $\lambda_1 = 195$ nm (see figure 15). At λ_0 the cinnamic acid side chains absorb, whereas the negative dichroism at λ_1 is due to the anisotropically distributed cyclobutane photoderivatives (see figures 14 and 15). This agreement with the linearly photopolymerized configuration is depicted in figure 14 [12]. Moreover, the two negative UV dichroism peaks at $\lambda_0 = 310$ nm and $\lambda_1 = 195$ nm in figure 15 suggest that the long axes of the cinnamic acid molecules as well as those of the cyclobutane molecules, which are both preferentially aligned perpendicular to $P_{\parallel}$ (see figure 14), induce liquid crystal director alignment $n \perp P_{\parallel}$ via dispersive interactions in linearly photopolymerized PVMC substrates. This may to some extent also hold for the σ electrons of the anisotropically elongated hydrocarbon main chains (see figure 14). On the other hand, the anisotropic main chain alignment in figure 14 may also lead to an anisotropy $\Delta\delta$ of the interatomic separation parameter parallel $P_{\parallel}$. $\Delta\delta \neq 0$ could occur (cf. equation (9)) if the alternating main chains and cyclobutane molecules in figure 14 led to microscopic density fluctuations parallel to $P_{\parallel}$. Since we have no evidence of surface roughness in our PVMC films, topological liquid crystal aligning forces are excluded [12].

As a molecular probe for testing the alignment of linearly photopolymerized substrates we used the strong and isolated infrared absorption band C≡N of alkenyl cyano liquid crystals such as:

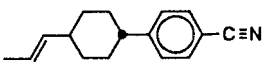

Since the longitudinal C≡N vibration at 2226 cm^{-1} is approximately parallel to the nematic director **n**, it is ideally suited for alignment tests.

Figure 16 shows part of the linearly polarized infrared transmission spectra of a 8 μm thick liquid crystal layer, sandwiched between two linearly photopolymerized PVMC-coated NaCl substrates [12]. The directions of linear UV curing **E**(LPP) on both substrates are identical (parallel). In figure 16, *P* is the analyser position of the IR spectrophotometer. From the strong, negative dichroism which the two spectra in figure 16 exhibit at 2226 cm^{-1}, it follows that the alignment of the C≡N bonds is (i) planar, (ii) uniaxial and (iii) perpendicular to **E**(LPP). This proves on a molecular level that parallel, linearly photopolymerized PVMC substrates indeed induce homogenous alignment in liquid crystals. The orientation of the nematic director $\mathbf{n} \perp \mathbf{E}$(LPP) which follows from figure 16, is identical to the direction of the slow optical axis of the linearly photopolymerized substrates (see figure 15).

5.2. *Performance of linearly photopolymerized substrates in liquid crystal displays*

Figure 17 shows the transmission versus voltage dependence of two twisted nematic liquid crystal displays with different substrates between crossed polarizers. Also shown are the corresponding voltage dependences of the twisted nematic liquid crystal display

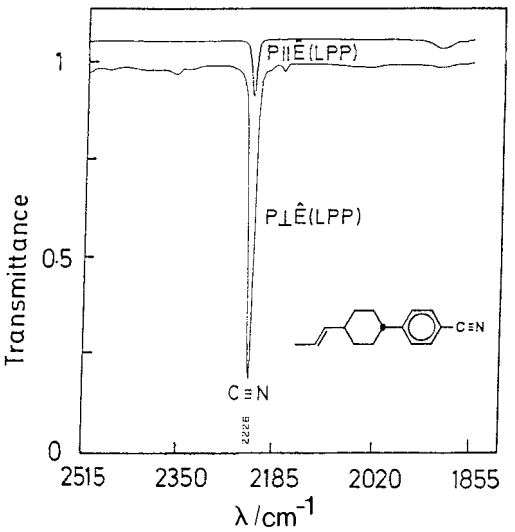

Figure 16. Part of the linearly polarized infrared transmission spectrum of an 8 μm thick liquid crystal layer sandwiched between two parallel, linearly photo-polymerized PVMC-coated NaCl substrates. $\mathbf{E}(\mathrm{LPP}) = \mathbf{E}_1(\mathrm{LPP}) = \mathbf{E}_2(\mathrm{LPP})$; where $\mathbf{E}$ = linearly polarized electric field of the UV curing light. The indices refer to the two liquid crystal display substrates. P = (linear) analyser position of the IR spectrophotometer. To distinguish the two spectra, the parallel spectrum is shifted upwards.

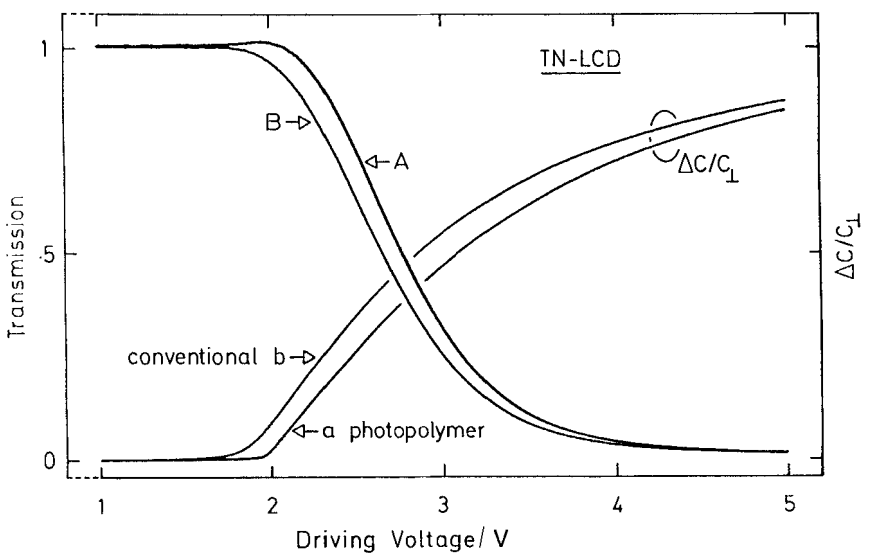

Figure 17. Transmission *versus* voltage, and capacitance *versus* voltage dependence $\Delta C/C_\perp$ of a linear photopolymerized aligned twisted nematic liquid crystal display (graphs A, a) and a conventionally aligned twisted nematic liquid crystal display (graphs B, b), at room temperature.

capacitance $\Delta C/C_\perp = (C_\parallel - C_\perp)/C_\perp$ [12]. Graphs a and A are recordings made with a twisted nematic liquid crystal display comprising one linearly photopolymerized aligning layer and one conventional aligning layer. Recordings b and B are made with a conventionally aligned twisted nematic liquid crystal display. Except for the different aligning layers, the twisted nematic liquid crystal displays are identical. The sharper initial slope of graph a at its capacitive threshold voltage $V_0(a) = 1{\cdot}90$ V, compared with the initial slope of graph b (see figure 17), indicates that linearly photopolymerized aligning layers induce smaller surface tilt angles than conventional polyimide aligned substrates. Both twisted nematic liquid crystal displays in figure 17 exhibit comparably large contrasts > 100. Since the linear photopolymerization aligning technique allows us to generate a director pattern $\mathbf{n}(\psi)$ with different azimuthal angles on the same substrate, twisted nematic configurations with different twist angles become possible in the same liquid crystal display. Figure 18 shows a hybrid liquid crystal display in which 90° twisted nematic areas (squares) are combined with homogeneously aligned areas on the same substrate [12]. The hybrid configuration is achieved by first linearly photopolymerizing the PVMC-coated substrate 1 of the liquid crystal display through a photomask in the x direction. After the completion of polymerization step 1, the polarization direction of the polymerizing UV light is rotated by 90°. Then, in a second step, the mask is removed and the area outside the squares is linearly polymerized in the y direction. This procedure leads to a liquid crystal alignment pattern on substrate 1 such that the nematic director $\mathbf{n}$ aligns within the squares in the y direction, whereas outside, the alignment is in the x direction. By combining substrate 1 with a conventionally, in the x direction aligned substrate 2, the hybrid liquid crystal display depicted in figure 18 is obtained; that is, the squares are twisted nematic liquid crystal displays, whereas the outside area is a parallel liquid crystal display configuration. Photographs A and B in figure 18 show the off-states of the hybrid liquid crystal display for the two polarizer configurations $\mathbf{n}_1 \| P_1 \| P_2$ (A) and $\mathbf{n}_1 \| P_1 \perp P_2$ (B). Since both, the twisted nematic region and the parallel region are virtually optically uniaxial in the z direction when 5 V are applied, both configurations are fully transparent in the on-state (not shown in figure 18).

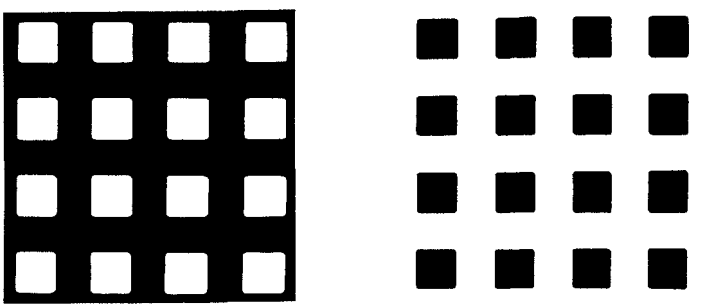

(a) (b)

$P_1 \| P_2$; $\mathbf{n}_1 \| P_1$; $V = 0$ V
squares: $\mathbf{n}_1 \| \mathbf{n}_2$
outside: $\mathbf{n}_1 \perp \mathbf{n}_2$ (twisted nematic)

$P_1 \| P_2$; $\mathbf{n}_1 \| P_1$; $V = 0$ V
squares: $\mathbf{n}_1 \perp \mathbf{n}_2$ (twisted nematic)
outside: $\mathbf{n}_1 \| \mathbf{n}_2$

Figure 18. Photograph of a hybrid liquid crystal display in its off-state between (A) parallel polarizers $P_1 \| P_2$ and (B) crossed polarizers $P_1 \perp P_2$. Cell gap $d = 6\,\mu$m liquid crystal-mixture = 6449 from F. Hoffmann-La Roche. Both liquid crystal display substrates are coated with non-patterned ITO electrodes. Within the $0{\cdot}5 \times 0{\cdot}5$ mm squares, the nematic directors are aligned in a twisted nematic configuration: $\mathbf{n}_1 \| P_1$, $n_2 \perp n_1$. Outside, the alignment is parallel: $\mathbf{n}_1 \| P_1$, $\mathbf{n}_2 \| \mathbf{n}_1$.

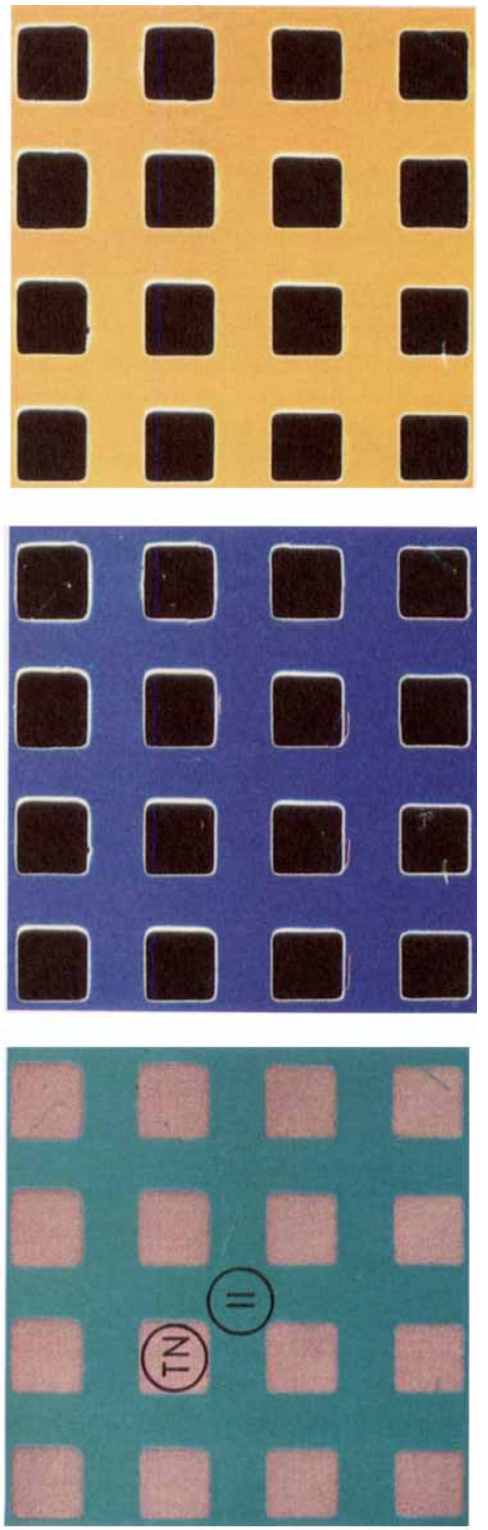

Figure 19. Voltage-dependent colour generation in the hybrid liquid crystal display of figure 18 when operated in the following polarizer configuration: $P_1 \perp P_2$ and ($\mathbf{n}_1$, P_1) = 45°. The driving voltages are 2·45 (A), 3·66 (B) and 5·07 V (C). The squares are TN-regions; the outside areas are parallel regions.

Figure 18 demonstrates that it is possible to generate optical patterns with linear photopolymerization aligned hybrid liquid crystal displays without patterning the liquid crystal display electrodes. By combining the linear photopolymerization aligning technique with patterned electrode configurations, many new possibilities to generate high resolution monochrome or colour images with liquid crystal displays become possible. In our experiments we achieved linear photopolymerization alignment patterns with a resolution better than 4 μm. The resolution was limited by the quality of the photomask.

Since $\mathbf{n}_1 \| P_1$ holds in the hybrid liquid crystal display of figure 18, both configurations A and B are black and white (see figure 18). That is, in both configurations, linear polarization is conserved within the liquid crystal layer. However, when rotating the crossed polarizers $P_1 \perp P_2$ in configuration B of figure 18 by 45°, elliptically polarized light is generated. Therefore, and because the ellipticity in the twisted nematic regions differs from the ellipticity in the parallel regions at the same driving voltage, different interference colours result. This converts the black-white hybrid liquid crystal display of figure 18 into the colour hybrid liquid crystal display shown in figure 19 [12].

Recently we have shown that linearly photopolymerized aligning layers perform well not only in parallel- and twisted nematic liquid crystal displays, but also in supertwisted nematic LCDs [12]. Apart from nematics, also ferroelectric liquid crystals can be aligned by linearly photopolymerized aligning layers. Because linearly photopolymerized aligned substrates do not require mechanical buffing, electrostatic charging cannot occur during the photo-generated aligning process. This eliminates the possibility of damaging the thin film transistors on actively addressable twisted nematic liquid crystal display substrates coated with linearly photopolymerized aligning layers. Moreover, the light-induced generation of birefringence patterns in liquid photopolymerization polymer layers which exhibit a variable direction of the slow optical axes, allows the integration of patterned optical retarders in liquid crystal displays, such as in supertwisted nematic liquid crystal displays. Thus, linear photopolymerization alignment and linear photopolymerization birefringence open up a vast number of new electro-optical and optical possibilities for liquid crystal displays (stereo-displays) as well as for fundamental studies of the complex interactions between anisotropic substrates and liquid crystals.

6. Ferroelectric liquid crystal displays and non-linear optic S_C^* liquid crystals

6.1. *Ferroelectric liquid crystal displays*

Since the discovery of ferroelectricity in chiral smectic C (S_C^*) liquid crystals by Meyer *et al.* [32] great efforts have been made to find electro-optical effects and suitable S_C^* liquid crystal materials rendering them applicable in liquid crystal displays. These efforts were intensified when Clark and Lagerwall suggested the use of the optical bistability of long pitch, Surface-stabilized ferroelectric liquid crystals in surface-stabilized ferroelectric displays [33]. One key requirement on ferroelectric liquid crystals for surface-stabilized ferroelectric liquid crystal displays is a helical pitch which is much longer than the cell gap. However, since the switching speed is directly proportional to the spontaneous polarization P_S, and because P_S decreases with increasing pitch, that is, with decreasing concentration of the chiral dopant, a conflicting situation occurs which makes the development of high speed liquid crystal

mixtures for surface-stabilized ferroelectric liquid crystal displays difficult. Furthermore, liquid crystal mixtures with large value of P_S destroy the bistability of surface-stabilized ferroelectric liquid crystal displays [34].

Figure 20 (*a*) shows the (ideal) bookshelf geometry of surface-stabilized ferroelectric liquid crystal display layers sandwiched between liquid crystal substrates [33]. The two stable orientations of the director field in the substrate plane result from switching the director on a cone which is determined by the angle 2θ, where θ is the tilt angle of the long molecular axes in the S_C plane. Switching occurs upon changing the polarity of the applied field, which causes the spontaneous polarization P_S of the ferroelectric liquid crystal layer to reverse direction. Because of the spontaneous polarization of S_C^* materials, short response times in the 50 μs range result for surface-stabilized ferroelectric liquid crystal displays at room temperature, i.e. two hundred times shorter

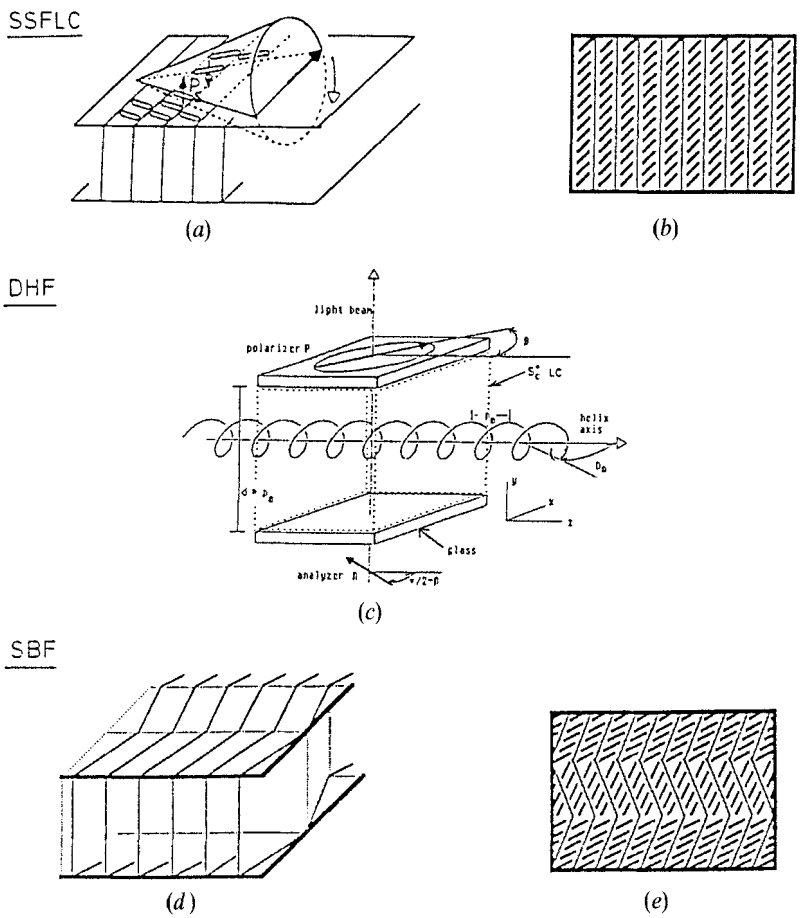

Figure 20. Ferroelectric liquid crystal configurations; (*a*) ideal bookshelf geometry of surface stabilized ferroelectric liquid crystal layer, (*b*) director orientation in substrate plane of surface stabilized ferroelectric liquid crystal display in one of its two bistable states, (*c*) deformed helical ferroelectric liquid crystal display in which helically twisted S_C^* planes are aligned perpendicularly to liquid crystal display substrates, (*d*) likely bookshelf geometry of short pitch ferroelectric configuration, (*e*) director orientation in substrate plane of short pitch bistable ferroelectric liquid crystal display in one of its two bistable states.

than the response of twisted nematic liquid crystal displays. Figure 20 (*b*) shows one of the two stable director orientations of surface-stabilized ferroelectric liquid crystals in the liquid crystal display substrate plane. The optical signal which the surface-stabilized ferroelectric effect generates between crossed linear polarizers is due to the change of the optical retardation upon switching the director between the two stable states. For a review of ferroelectric liquid crystals see [2, 35].

The inherent difficulty of generating grey levels with optically bistable ferroelectric liquid crystal displays was recently overcome by Beresnev *et al.* [36] who discovered a linear electro-optical effect in ferroelectric liquid crystals which is based on the field-induced deformation of a helical ferroelectric configuration in short pitch S_C^* liquid crystal layers. Figure 20 (c) schematically shows a deformed helical ferroelectric liquid crystal display. As a consequence of the helix deformation upon applying a voltage to the deformed helical ferroelectric liquid crystal display, the index ellipsoid of the S_C^* layer rotates in the xz plane and the liquid crystal display transmission changes linearly with increasing voltage. Because of the almost ideally large tilt angle $\theta \cong 45°$ of deformed helical ferroelectric liquid crystal displays, their off-state brightness reaches the desired 100 per cent [37]. Deformed helical ferroelectric liquid crystal displays require low operating voltages $V < 2$ V and achieve, by actively addressing them, large multiplexing rates and response times in the 10 μs range. The short response times are due to the large P_s values that can be designed into deformed helical ferroelectric liquid crystals without adversely affecting the performance of the display [37]. Besides from the optically bistable surface stabilized ferroelectric liquid crystal display of Clark and Lagerwall and the tristable effect by Chandani *et al.* [38], Fünfschilling and Schadt recently described a new optically bistable ferroelectric S_C^* configuration which requires, like the deformed helical ferroelectric effect, short pitch ferroelectric liquid crystals [39]. Prerequisites for their short pitch bistable ferroelectric effect are ferroelectric S_C^* materials which exhibit—unlike surface stabilized ferroelectric materials—a large spontaneous polarization $P_S \sim 60\,\text{nC}\,\text{cm}^{-2}$ and a short pitch $p \lesssim 0{\cdot}4\,\mu\text{m}$. The quasi-bookshelf molecular configuration of a field aligned short pitch bistable ferroelectric liquid crystal display is depicted in figure 20 (*d*), whereas figure 20 (*e*) shows one of the two stable director configurations in the plane of the short pitch bistable ferroelectric liquid crystal display substrate [2, 39]. Short pitch bistable ferroelectric liquid crystal displays exhibit very short switching times, below 25 μs at room temperature, and optimal memory switching angles. As in surface stabilized ferroelectric liquid crystal displays, the electro-optical effect of short pitch bistable ferroelectric liquid crystal displays is due to a rotation of the index ellipsoid of the birefringent liquid crystal layer in the plane of the cell. Therefore, thin cells with an optical retardation $\Delta nd = 0{\cdot}27\,\mu\text{m} \simeq \lambda/2$ are required to obtain black-white images. However, in contrast to surface stabilized ferroelectric liquid crystal displays, the cell gap of short pitch bistable ferroelectric liquid crystal displays can easily be increased in those applications which tolerate a restricted spectral range (for example colour projection system). Like surface stabilized ferroelectric liquid crystal displays, short pitch bistable ferroelectric liquid crystal displays are sufficiently bistable to allow for virtually infinite multiplexing rates [39]. However, contrary to surface stabilized ferroelectric liquid crystal displays, the short pitch bistable ferroelectric configuration can be field aligned which allows curing of dislocations in the display during operation.

Like for deformed helical ferroelectric liquid crystal displays, large spontaneous polarization can be designed into short pitch bistable ferroelectric liquid crystal displays (SBFFLCs) without adversely affecting the optical appearance of the display.

This compatibility between large P_S and optical bistability is important not only to achieve fast responding, high contrast short pitch bistable ferroelectric liquid crystal displays, it will also become important for realizing (bi)stable ferroelectric non-linear optical devices with non-linear optical ferroelectric liquid crystals such as with the new materials presented next.

6.2. *Strongly non-linear optical S_C^* liquid crystals*

Prerequisites for generating second harmonics in a dielectric by the electric field of an incident light wave of frequency ω are (i) a non-vanishing second order susceptibility χ_2 in the series expansion of the macroscopic polarizability P of the dielectric and (ii) a non-centrosymmetric crystal structure which prevents averaging out the second order molecular hyperpolarizabilities on a macroscopic scale. For details on non-linear optics see [40, 41]. Apart from these basic requirements, quite a number of other crucial conditions must be met by a dielectric to qualify for practical applications in integrated optics devices, such as in frequency converters or electro-optical modulators (Pockels effect). Thus, wave-guiding in thin films of the dielectric must be possible and the non-linear optical efficiency must not only be large but also stable. Whereas wave-guiding requires optically anisotropic dielectrics, one prerequisite for stability is a stable, non-centrosymmetric lattice structure.

The macroscopic polarizability P of an isotropic dielectric can be expressed in a series expansion [40]

$$P = \varepsilon_0(\chi E + \chi_2 E^2 + \chi_3 E^3 + \ldots). \tag{10}$$

Pictorially figure 21 illustrates the molecular hyperpolarizability of the π electrons in an aromatic donor-acceptor ring system [41]: The stronger the donor–acceptor push–pull action, the larger become the principal dipole moment and χ_2. The donor–acceptor groups NH_2 and NO_2 define the principal non-linear optical axis which is parallel to the principal diopole moment (see figure 21). Because of their large design flexibility,

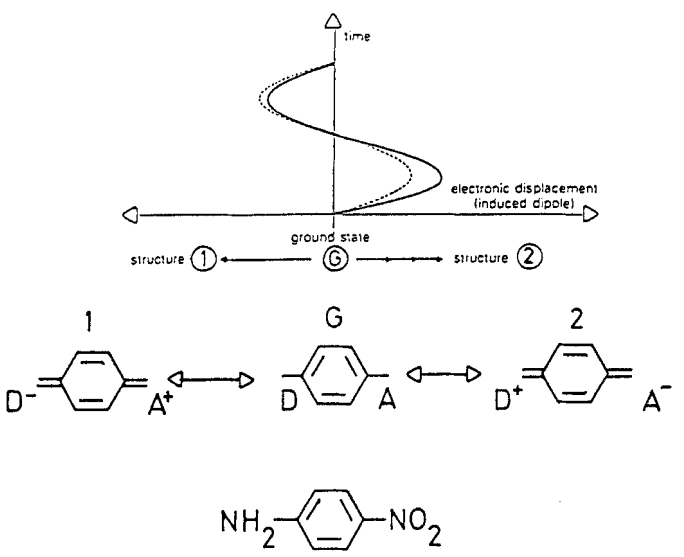

Figure 21. Pictorial non-linear optical activity of a highly conjugated donor–acceptor molecule.

organic materials, whose molecules can be engineered such that they exhibit specific long range order, are very interesting candidates for novel non-linear optical materials, provided that efficient, non-centro-symmetric and stable molecular configurations are found.

Because of the non-centrosymmetric (C2) polar symmetry of ferroelectric liquid crystal configurations (see figures 20(*a*) and (*d*) ferroelectric liquid crystals are interesting candidates for second harmonic generation. Moreover, because of their optical anisotropy and because ferroelectric liquid crystals can be uniformly ordered in thin layers, the prerequisites for wave-guiding in integrated optics devices are also given. Unfortunately, the second harmonic generation efficiency of most ferroelectric liquid crystals investigated so far is orders of magnitude below that of state of the art inorganic crystals, such as lithium niobate $LiNbO_3$ [42]. For a recent review on second harmonic generation in ferroelectric liquid crystals see [43]. So far the largest second harmonic generation coefficient $d_{22} = \chi_2/2$ (see equation (10)) reported for ferroelectric liquid crystals is $d_{22} = 0{\cdot}6\,\text{pm V}^{-1}$ [44].

In this paper we present novel, highly efficient non-linear optical ferroelectric liquid crystal materials whose second harmonic generation properties were investigated in 13 μm thin, homeotropically aligned layers [1]. To achieve an S_C^* phase with large values of spontaneous polarization and to allow for efficient phase matching in planar ferroelectric liquid crystals configurations, such as in those of figures 20(*a*) and (*d*), the second harmonic generation active nitroaniline groups are laterally arranged in our new molecules:

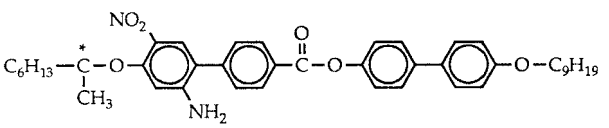

Positioning the chiral centre in the alkoxy terminal chain adjacent to the nitroaniline dipole moment strongly enhances both P_S and the second harmonic generation efficiency. This design concept leads, with $d_{22} = 5\,\text{pm V}^{-1}$, to the largest second harmonic generation coefficients reported so far for ferroelectric liquid crystals [1]. Actually this value is not too far off d_{33} ($LiNbO_3$) $\simeq 30\,\text{pm V}^{-1}$ [41], the best of inorganic second harmonic generation materials. Moreover, because the new non-linear optical ferroelectric liquid crystal materials possess glass transition temperatures T_g below their S_C^* mesophases, their non-linear optical active, polar C2 configurations in the S_C^* phase can be perfectly preserved by operating them below T_g. Thus, efficient and stable configurations result.

7. Conclusions

Liquid crystals and liquid crystal displays are a consequence of the anisotropic molecular long range interactions which induce the molecular-specific order phenomena typical for mesomorphic compounds. Apart from intermolecular interactions among themselves, liquid crystal molecules are able to anisotropically interact sterically or via dispersive forces with substrates. Both types of interaction, which are not independent, can be combined in macroscopically ordered organic layers such that predetermined symmetries result. Liquid crystal displays are examples of electro-optical devices in which effect-specific boundary conditions are combined with effect-specific functional liquid crystals.

The material and electro-optical properties of novel, halogenated nematic alkenyl liquid crystals, comprising a number of different functional groups, are correlated. Synergisms between them lead to low viscosities, broad nematic mesophases and large dielectric anisotropies. The highly resistive materials are designed for actively addressed twisted nematic liquid crystal displays. Moreover, it is shown that dislocation-free, planar cholesteric optical filters for liquid crystal display projectors can be achieved by field-alignable, negative dielectric anisotropic, short pitch cholesterics.

An example which exemplifies anisotropic liquid crystal substrate interactions is given by novel photopolymers which become optically anisotropic upon polymerization with linearly polarized light. The dispersive anisotropies which result are shown to induce uniaxial, planar alignment of liquid crystals in contact with the linearly photopolymerized polymer substrates. The new linearly photopolymerized liquid crystal aligning technique allows us to create a high resolution director pattern with arbitrary azimuthal angles on the same substrate. This opens up interesting possibilities for realizing new optical and electro-optical devices. Thus, different electro-optical effects can be combined on the same liquid crystal display substrate and the generation of stereo–liquid crystal display images becomes feasible. Linearly photopolymerized alignment avoids mechanical brushing and damaging of actively addressable liquid crystal display substrates.

Other examples where use can be made of the broad functionality of organic molecules and of the potential to affect the symmetry of layers of mesomorphic compounds, by combining molecular-specific symmetries with proper boundary conditions, are non-linear optical materials and devices. Novel non-linear optical ferroelectric liquid crystals recently developed in our laboratories exhibit the largest second order harmonic coefficients reported so far. They approach those of state of the art inorganic crystals ($LiNbO_3$) and they are stable. The design of the non-linear optical ferroelectric liquid crystals is such that waveguiding operation is possible, thus rendering them applicable in integrated optical devices, such as in frequency converters and gigahertz optical modulators.

The intention of the diverse content of this plenary article is to illustrate the fascinating technological potential which follows from combining modern molecular material design principles based on highly ordered organics, with device applications. This leads to interesting and more and more diversified applications not only within the liquid crystal display technology, but also directed towards new technologies, such as integrated optics.

It is a pleasure to acknowledge the many fruitful discussions and the skilled experimental work of my collaborators Richard Buchecker, Carsten Benecke, Jürg Fünfschilling, Rolf-Peter Herr, Steven Kelly, Klaus Schmitt, Herbert Seiberle and Alois Villiger as well as the fruitful collaboration with Vladimir Kozinkov and Vladimir Chigrinov from NIOPIK, Moscow, on linearly photopolymerized alignment of liquid crystals.

References

[1] SCHMITT, K., HERR, R. P., SCHADT, M., FÜNFSCHILLING, J., BUCHECKER, R., CHEN, X. H., and BENECKE, C., 1993, *Liq. Crystals*, **14**.

[2] SCHADT, M., 1992, *Displays*, **13**, 11.

[3] FÜNFSCHILLING, J., 1991, *Condensed Matter News*, **1**, 12.

[4] SCHADT, M., and HELFRICH, W., 1970, *Appl. Phys. Lett.*, **18,** 127.
[5] SCHEFFER, T., and NEHRING, J., 1984, *J. appl. Phys.*, **45,** 1021.
[6] SCHADT, M., 1991, *Proc. S.P.I.E.*, **1455,** 214.
[7] SCHADT, M., and FÜNFSCHILLING, J., 1990, *Jap. J. appl. Phys.*, **29,** 1974.
[8] SUGIMORI, S., 1990, German Offenlegungschrift DE 3102017C2.
[9] FINKENZELLER, U., KURMEIER, A., and POETSCH, E., 1989, *Proceedings Freiburger Arbeitstagung.*
[10] SCHADT, M., BUCHECKER, R., and VILLIGER, A., 1990, *Liq. Crystals*, **7,** 519.
[11] SUGIYAMA, T., KUNIYASU, S., SEO, D., FUKURO, H., and KOBAYASHI, S., 1990, *Jap. J. appl. Phys.*, **29,** 2045.
[12] SCHADT, M., SCHMITT, K., KOZINKOV, V., and CHIGRINOV, V., 1992, *Jap. J. appl. Phys.*, **31,** 2155.
[13] SEIBERLE, H., and SCHADT, M., 1992, *Digest*, S.I.D., **92,** 25.
[14] SCHADT, M., BUCHECKER, R., and MÜLLER, K., 1989, *Liq. Crystals*, **5,** 293.
[15] SCHADT, M., BUCHECKER, R., VILLIGER, A., and KELLY, S., 1992, *Liq. Crystals* (to be published).
[16] BOLLER, A., CEREGHETTI, M., SCHADT, M., and SCHERRER, H., 1977, *Molec. Crystals. liq. Crystals*, **42,** 215.
[17] SCHAD, HP., and OSMAN, M. A., 1981, *J. chem. Phys.*, **75,** 880.
[18] LEADBETTER, A. J., RICHARDSON, R. M., and COLLING, J., 1975, *J. Phys. Colloq., Paris*, **36,** 37.
[19] KELLY, S. M., 1991, *Liq. Crystals*, **10,** 261.
[20] SCHIEKEL, N. S., and FAHRENSCHON, K., 1971, *Appl. Phys. Lett.*, **19,** 391.
[21] BELAYEV, S. V., SCHADT, M., BARNIK, M. I., FÜNFSCHILLING, J., MALIMONEKO, N. V., and SCHMITT, K., 1990, *Jap. J. appl. Phys. Lett.*, **29,** 273.
[22] HAMADA, H. FUNADA, F., HIJIKIGAWA, M., and AWANE, K., 1992, *Digest S.I.D.* **92,** 269.
[23] CHANDRASEKHAR, S., 1977, *Liquid Crystals* (Cambridge Monographs on Physics).
[24] ALT, P. M., and PLESHKO, P., 1974, *Trans. Electron Dev.*, **ED-21,** 146.
[25] PROST, J. E., and TER-MINASSIAN-SARAGA, 1975, *J. Phys.*, **36,** CI-77.
[26] OKANO, K., and MURAKAMI, J., 1979, *J. Phys.*, **40,** C3-525.
[27] HALLER, I., 1974, *Appl. Phys. Lett.*, **24,** 349.
[28] BERREMAN, D. W., 1972, *Phys. Rev. Lett.*, **28,** 1683.
[29] GEARY, J. M., GOODBY, J. W., KMETZ, A. R., and PATEL, J. S., 1987, *J. appl. Phys.*, **62,** 4100.
[30] ISHIHARA, S., WAKEMOTO, H., NAKAZIMA, K., and MATSUO, Y., 1989, *Liq. Crystals*, **4,** 669.
[31] BERNASCONI, J., STRÄSSLER, S., and ZELLER, H. R., 1980, *Phys. Rev.* A, **22,** 276.
[32] MEYER, R. B., LIEBERT, L., STRZELECKI, L., and KELLER, P., 1975, *J. Phys., Paris*, **36,** L69.
[33] CLARK, N. A., and LAGERWALL, S. T., 1980, *Appl. Phys. Lett.*, **36,** 899.
[34] YANG, K. H., and CHIEN, T. C., 1989, *Jap. J. appl. Phys.*, **28,** L1599.
[35] FUKUDA, A., ONICHI, Y., ARAI, H., TAKANO, H., ISHIKAWA, K., and TAKEZOE, H., 1989, *Liq. Crystals*, **5,** 1055.
[36] BERESNEV, L. A., CHIGRINOV, V. G., DERGACHEV, D. I., POSHIDAEV, E. P., FÜNFSCHILLING, J., and SCHADT, M., 1989, *Liq. Crystals*, **5,** 1171.
[37] FÜNFSCHILLING, J., and SCHADT, M., 1990, *Jap. J. appl. Phys.*, **66,** 3877.
[38] CHANDANI, A. D. L., GORECKA, E., OUCHI, Y., TAKAZOE, H., and FUKUDA, A., 1989, *Jap. J. appl. Phys.*, **28,** L1265.
[39] FÜNFSCHILLING, J., and SCHADT, M., 1991, *Jap. J. appl. Phys.*, **30,** 741.
[40] BLOEMBERGER, N., 1965, *Non-linear Optics* (Benjamin).
[41] CHEMLA, D. S., and ZYSS, J., 1987, *Non-linear Optical Properties of Organic Molecules and Crystals*, vol. 1 (Academic Press).
[42] WEBER, M. J., 1986, *CRC Handbook of Laser Science and Technology*, vol. III (CRC Press).
[43] DREVENSEK, I., and BLINC, R., 1992, *Condensed Matter News*, **1,** 14.
[44] LIU, J. Y., ROBINSON, M. G., JOHNSON, K. M., and WALBA, D. M., 1991, *J. appl. Phys.*, **70,** 3426.